THE EFFECTS OF LOW-FREQUENCY SPICINESS ANOMALIES ON THE EL-NIÑO - SOUTHERN OSCILLATION

A THESIS SUBMITTED TO THE GRADUATE DIVISION OF THE
UNIVERSITY OF HAWAI‘I AT MĀNOA IN PARTIAL FULFILLMENT
OF THE REQUIREMENTS FOR THE DEGREE OF

MASTER OF SCIENCE

IN

OCEANOGRAPHY

DECEMBER 2013

By
Louis Michael Grissom Jr.

Thesis Committee:

Niklas Schneider, Chairperson
Axel Timmermann
Bo Qui

We certify that we have read this thesis and that, in our opinion, it is satisfactory in scope and quality as a thesis for the degree of Master of Science in Oceanography.

THESIS COMMITTEE

_____
Chairperson

_____

_____

For my wife Valerie and my son Michael Kai

Acknowledgments

This work would not be possible without the help and support of many people. Primarily, I would like to thank my family for all the support throughout my life. They have helped me to become the person I am today. A special thanks goes to my wife Valerie for encouraging me to pursue graduate studies and making me believe that anything is possible.

I am also indebted to the many people of the oceanography department, from the administrative staff to the many great professors. I would like to thank my committee members Axel Timmerman and Bo Qiu for their help and feedback during my graduate studies and research, and Eric Firing for the many lessons in physical oceanography and for teaching me to be precise when I speak. I would especially like to thank my graduate advisor Niklas Schneider for being a great, great mentor and an overall great person. His approach to advising is exemplary and I have enjoyed our many conversations. My days at sea with the Hawaiian Ocean Time-series were also a great experience and I'd like to thank Fernando Santiago-Mandujano and Jeffrey Snyder for teaching me hands-on oceanography.

Support for this work was provided through Scientific Discovery through Advanced Computing (SciDAC) program funded by U.S. Department of Energy, Office of Science, Advanced Scientific Computing Research under award number DE-SC0005111.

Abstract

Low-frequency subsurface spiciness anomalies generated in the northern and southern subtropics of the Pacific Ocean advect geostrophically westward and equatorward where they often enter the equatorial undercurrent (EUC). Assuming the spiciness anomalies in each hemisphere are generated independently, the temperature gradient across the pycnocline, $\partial T/\partial \rho$, may vary significantly on decadal time scales in the EUC as a result of convergent spiciness anomalies. Observations of $\partial T/\partial \rho$ from an eight-year time series of Argo float profile data show variability around the mean value of approximately 10% in the warm pool region where the EUC forms. Decadal variability may be significantly larger. As spiciness anomalies propagate east in the EUC, they may affect the sea surface temperature in the cold tongue region, which is sensitive to the subsurface temperature and vertical displacements of the pycnocline. Using a modified Zebiak-Cane ENSO model, the effect of $\partial T/\partial \rho$ variability on ENSO is studied. Results show that $\partial T/\partial \rho$ variability in the NINO3 region similar to that shown by Argo observations has a significant affect on ENSO variance; as $\partial T/\partial \rho$ increases (decreases), ENSO variance increases (decreases). This result is primarily due to an increase in the growth rate of ENSO resulting from an increase in the sensitivity of the thermocline feedback and the non-linearity of the system. These results indicate that for accurate forecasting of ENSO, low-frequency spiciness variability in the subtropical and western equatorial Pacific should be considered.

Table of Contents

List of Figures

Chapter 1

Introduction

The El Niño-Southern Oscillation (ENSO) is the dominant mode of tropical climate variability on interannual timescales. As such, the characteristics and mechanisms that underly the phenomenon have been investigated thoroughly for many years. The canonical ENSO event has a period between 3-7 years, sea surface temperature (SST) anomalies at the height of El Niño are typically 3-5 degrees Celsius, and the center of action, or the location of largest SST anomalies, is usually in the eastern tropical Pacific (Rasmusson and Carpenter, 1982).

Superimposed on the interannual variability of ENSO is variability on decadal timescales (Trenberth and Hoar, 1996; Fedorov and Philander, 2001). Between 1960 and 1980, the period of ENSO was of short duration with an average period of approximately three years. Since the 1980's, the oscillation has spent proportionally less time in the La Niña phase, the average period has increased to around five years, and the two strongest El Niño events on record have occurred. This decadal variability not only includes the dominant phase and period of ENSO , but also whether the center of action of El Niño lies in the eastern tropical Pacific or more towards the central tropical Pacific (Trenberth and Stepaniak, 2001; Larkin and Harrison, 2005; Yu and Kao, 2007; Kao and Yu, 2009; Ashok, Behera, Rao, Weng and Yamagata, 2007; Kug, Jin and An, 2009).

El Niño events that have large SST anomalies in the central Pacific with SST anomalies in the eastern Pacific less pronounced have been called by many names. Larkin and Harrison (2005) referred to them as Dateline El Niño because of the proximity of the maximum SST anomalies to the international date line. Ashok et al. (2007) used the phrase El Niño Modoki to describe the spatial pattern of the second empirical orthogonal function (EOF) of monthly tropical Pacific SST which showed maximum SST variance in the central Pacific. Interestingly, the authors compared the years 1958-1978 and 1979-2004 and showed that El Niño Modoki has occurred more frequently in recent decades. They attribute this occurrence to the recent weakening of the trade winds due to

a weaker zonal temperature gradient, leading to a flatter equatorial thermocline. Both Larkin and Harrison (2005) and Ashok et al. (2007) demonstrate that the global teleconnections associated with this type of El Niño event are distinct from those of the conventional version.

The decadal changes documented in the ENSO cycle bring many questions to mind. Why has the La Niña phase been less active since the 1980's? Why has the occurrence of El Niño Modoki increased in recent decades, and what are the oceanic and atmospheric processes responsible for its development? To seek the answers to these questions, many researchers have looked to the subtropics for a possible link (Gu and Philander, 1997; Schneider, Miller, Alexander and Deser, 1999). In the Pacific, central and eastern subtropical surface water is subducted into the pycnocline where it advects nearly adiabatically along geostrophic pathways westward and toward the equator. Once at the equator, the water mass moves east in the Equatorial Undercurrent (EUC), upwells to the surface and then returns poleward via Ekman drift. This shallow upper ocean circulation is called the subtropical cell (STC) and is an important vehicle for meridional heat transport (McCreary and Lu, 1994).

The STC's equatorward lower branches can be divided into a western boundary pathway (WBP) that passes through the low-latitude western boundary currents while heading to the equator and an interior pathway (IP) that takes a more direct route through the central basin. Goodman, Hazeleger, de Vries and Cane (2005) found that three quarters of the subtropical trajectories that terminate in the EUC take the WBP, while the remainder take the IP. In addition, the transport by the IP is typically weaker than that of the WBP by a factor of two to three but exhibits stronger interannual and decadal variability (Johnson and McPhaden, 1999; Huang and Wang, 2001; Wang and Huang, 2005). Huang and Wang (2001) found that the interior pathway varies on interannual and decadal timescales in terms of both mass transport and longitudinal location, depending largely on the strength of the low latitude zonal winds. An ENSO signature was also noted by the authors in that the IP width had a larger (smaller) latitudinal span during La Niña (El Niño) years.

A hemispheric asymmetry exists in the Pacific between both the mass flux of the IP and WBC to the EUC and the share of the EUC source waters. The South Pacific contributes as much as 70% of the source water to the EUC (Blanke and Raynaud, 1997; Goodman et al., 2005). The hemispheric disparity in the EUC source waters is partly due to the Indonesian Throughflow preferentially taking water from the North Pacific (Gordon and Fine, 1996) and partly due to the presence of the Inter-Tropical Convergence Zone (ITCZ) in the North Pacific which blocks a portion of the interior transport from the subtropical North Pacific to the equatorial Pacific by forming a potential vorticity barrier (Lu and McCreary Jr, 1995). The negative wind stress curl associated with the

ITCZ generates upward Ekman pumping and reduces isopycnal layer thickness. Since potential vorticity is largely conserved in the subsurface ocean and relative vorticity is low where isopycnal layer thickness is small, water parcels cannot travel further south as the isopycnal layer thickness increases just south of the ITCZ. The climatological position of the South Pacific Convergence Zone (SPCZ) is in the western South Pacific and it's eastern edge rarely lies east of 140W (Vincent, Lengaigne, Menkes, Jourdain, Marchesiello and Madec, 2011). As such, the interior transport in the South Pacific is not hindered by the SPCZ and therefore is larger than the interior transport in the North Pacific.

Gu and Philander (1997) were the first to suggest that the STC plays a role in decadal tropical variability, whereby SST anomalies subduct at subtropical latitudes, are advected by the mean flow in the lower branch of the STC, and upwell in the cold tongue of the eastern tropical Pacific and affect air-sea interaction. The SST anomaly of subtropical origin amplifies an initial anomaly in the cold tongue and the ensuing atmospheric response is to generate zonal wind anomalies in the subtropics that generate an opposite-signed SST anomaly that subducts, completing a decadal cycle.

Since the geostrophic advection of water masses in the subsurface is generally along isopycnal surfaces, density compensated temperature and salinity anomalies, or spiciness, is an important variable of water masses subducting and propagating in the subtropical cell. Some fraction of a temperature anomaly will affect water density and thus will affect, and be affected by, planetary wave dynamics. Meanwhile, the remaining fraction will be density-compensated by salinity anomalies and will advect as a passive tracer. This density-compensated fraction is the spiciness anomaly, with warm and salty (cool and fresh) anomalies having high (low) spiciness (Munk, 1981).

Using a 130-year integration of a coupled ocean-atmosphere global circulation model, Schneider (2000) found a decadal spiciness mode in the tropics involving anomalous advection on subsurface isopycnals due to anomalous wind stress curl over mean subsurface temperature gradients. In a further study, Schneider (2004) demonstrated that the emergence of subsurface spiciness anomalies in the central equatorial Pacific initiates a delayed, negative feedback with the subtropical North Pacific and a positive feedback with the equatorial and subtropical South Pacific.

Observational studies (Deser, Alexander and Timlin, 1996; Schneider et al., 1999; Sasaki, Schneider, Maximenko and Lebedev, 2010) as well as modeling studies (Zhang, Kagimoto and Zebiak, 2001) have shown the subduction and propagation of decadal temperature anomalies in the North Pacific thermocline , but the arrival of these anomalies to the eastern equatorial Pacific has yet to be demonstrated. Furthermore, Nonaka, Xie and Takeuchi (2000) have shown that a passive tracer originating from the eastern North Pacific may not arrive at the eastern equatorial Pacific

with any appreciable magnitude. Tailleux, Lazar and Reason (2005) point out that the amplitude modulation of subsurface spiciness signals propagating from the subtropical North Pacific to the equatorial region can have a significant attenuation factor of 0.72. They attribute this effect primarily to the difference in the ratio of the coefficients of haline contraction and thermal expansion between the subtropics and equatorial region. Despite these results and given the interannual and decadal variability of the North Pacific interior pathway (Johnson and McPhaden, 1999; Huang and Wang, 2001; Wang and Huang, 2005), the propagation of decadal spiciness anomalies from the North Pacific to the eastern equatorial Pacific cannot be ruled out as a component of decadal climate variability.

In the South Pacific, decadal spiciness anomalies have been shown to affect the equatorial region. In the absence of a potential vorticity barrier like that in the North Pacific, the subsurface waters of the South Pacific can communicate more effectively with the equator. In fact, Giese, Urizar and Fučkar (2002) implicate decadal spiciness originating from the South Pacific and upwelling in the equatorial region as part of the 1976 climate shift. Other modeling studies have also demonstrated the effectiveness of the South Pacific to generate and communicate spiciness anomalies to the equator (Yeager and Large, 2004; Nonaka and Sasaki, 2007; Luo, Rothstein, Zhang and Busalacchi, 2005). Using a global ocean GCM with 40 year realistic surface forcing, Yeager and Large (2004) showed spiciness anomalies on the 25.5σ isopycnal propagating from the eastern North Pacific and eastern South Pacific westward and equatorward along mean geostrophic pathways. A region of high spiciness variance was noted as the anomalies converged in the equatorial western Pacific after passing through the western boundaries. They proposed a subsurface injection mechanism at work in the eastern subtropical Pacific that generates positive (warm and salty) spiciness anomalies during deep winter mixing in regions with strong vertical salinity gradients and weak density stratification, and demonstrated this mechanism at work in a further study using observational data (Yeager and Large, 2007). Johnson (2006) also demonstrated the formation of spiciness in this region using Argo float observations.

As spiciness anomalies from both hemispheres converge on the equator, they can act to sharpen or weaken the temperature gradient across the pycnocline depending on whether they are of the same or opposite sign and what isopycnal they are on. Convergence can occur in the western equatorial Pacific for anomalies that have passed through the western boundary region or further east in the EUC for those that take an interior pathway, or a combination of the two. On decadal timescales, spiciness anomalies generated in the subtropics and propagating into the EUC may

alter the SST structure and ENSO character. In this thesis, this hypothesis will be investigated using observational data and experiments in an intermediate complexity discharge-recharge ENSO model.

Much of the prior research on the link between the subtropical and tropical Pacific involving spiciness anomalies has depended on limited observations or modeling studies. While modeling provides invaluable insight into these processes, observational evidence is perhaps more valuable. With the advent of the global array of drifting Argo floats it is now possible to study the formation and propagation of spiciness with observations of unprecedented spatial coverage. Using these data, this thesis will explore the spiciness signal that is present in the Argo observations in the Pacific with the goal of determining the extent to which spiciness anomalies in the Pacific propagate toward the equator where they may enter the EUC. Insight from the Argo observations will then feed into experiments with a modified version of the intermediate coupled ocean-atmosphere model used by Zebiak and Cane (1987), hereafter called the MZC model. The thesis is organized as follows. Chapter Two will analyze the Argo data for decadal spiciness variability, Chapter Three will discuss experimental results from the MZC model, and Chapter Four will present a summary and conclusions.

Chapter 2

Spiciness in the Argo Data

2.1 Data and Methods

In this chapter I use two products derived from the vertical profiles of in-situ temperature and salinity from the network of drifting Argo floats. The profiles from the period January 2005 to December 2012 are obtained from the US Global Argo Data Assembly Center by the Asia-Pacific Data-Research Center (APDRC) at the University of Hawaii at Manoa, who then use the profiles to compute potential temperature and potential density using a locally linearized equation of state (see http://apdrc.soest.hawaii.edu/projects/ Argo/data/Documentation/gridded-var.pdf). These profiles are then interpolated onto 27 standard depth levels from the surface to 2000m with a vertical resolution that is relatively fine (25-50m) in the upper 500m that will be studied here.

In addition, a second product turns these vertically interpolated data into a horizontally gridded product using a variational interpolation algorithm. The principle of the technique is to minimize the misfit between the interpolated fields on the grid and the irregularly distributed observational data. The horizontal resolution of the gridded data is 1 degree in latitude and longitude globally with a monthly time resolution.

Although a spiciness calculation is provided by APDRC in this product, I compute spiciness from the potential temperature and potential density fields following Taguchi and Schneider (2013). To split temperature anomalies into a density-compensated component (spiciness) and a component that alters the water density, we first represent the anomalous temperature and density fields as a displacement from the long term mean field as

$$T(\vec{x}) = \overline{T}(\vec{x} - d\vec{x}) \tag{2.1.1}$$

$$\rho(\vec{x}) = \overline{\rho}(\vec{x} - d\vec{x}) \tag{2.1.2}$$

where $\vec{x}$ is the three-dimensional position vector, $d\vec{x}$ is the displacement vector, and $\overline{T}$ and $\overline{\rho}$ are the time mean fields of temperature and density, respectively. For displacements small compared to the ratio of gradient and curvature of temperature and density, anomalies can be written as

$$dT = -\nabla\overline{T} \cdot d\vec{x} \tag{2.1.3}$$

$$d\rho = -\nabla\overline{\rho} \cdot d\vec{x} \tag{2.1.4}$$

Temperature anomalies can be split into components related to density changes and spiciness as

$$dT = dT_\rho + dT_\chi \tag{2.1.5}$$

and the displacement vector can be split into components aligned and parallel to the density gradient as

$$d\vec{x} = d\vec{x}_\rho + d\vec{x}_\chi = \left(d\vec{x} \cdot \frac{\nabla\overline{\rho}}{|\nabla\overline{\rho}|}\right)\frac{\nabla\overline{\rho}}{|\nabla\overline{\rho}|} + d\vec{x}_\chi \tag{2.1.6}$$

Combining equations (2.1.3) and (2.1.6) gives the two components of the temperature anomaly as

$$dT = -\left(\nabla\overline{T} \cdot \frac{\nabla\overline{\rho}}{|\nabla\overline{\rho}|}\right)\frac{\nabla\overline{\rho} \cdot d\vec{x}}{|\nabla\overline{\rho}|} - \nabla\overline{T} \cdot d\vec{x}_\chi \tag{2.1.7}$$

or using equation (2.1.4) we have

$$dT = \left(\nabla\overline{T} \cdot \frac{\nabla\overline{\rho}}{|\nabla\overline{\rho}|^2}\right)d\rho - \nabla\overline{T} \cdot d\vec{x}_\chi = dT_\rho + dT_\chi \tag{2.1.8}$$

The spiciness component can then be isolated by subtraction of the density-altering component of temperature anomalies from the total anomaly as

$$dT_\chi = dT - dT_\rho = dT - \left(\nabla\overline{T} \cdot \frac{\nabla\overline{\rho}}{|\nabla\overline{\rho}|^2}\right)d\rho \tag{2.1.9}$$

To quantify the total spiciness anomaly in the pycnocline at a given location it is useful to perform a depth integration of equation (2.1.9) over the depth intervals of the upper ocean subsurface flow followed by a long term mean calculation. Here the depth interval is taken to be 50-400 meters. The surface mixed layer processes are avoided by exclusion of the top 50 meters. Since spiciness anomalies in the pycnocline are advected by the slow subsurface flow, a one year mean of the depth integration shows the spiciness propagation quite well.

2.2 Propagation of Spiciness Anomalies

Strong spiciness formation regions exist where sharp unstable vertical salinity gradients are found in regions of deep winter mixing and unstable stratification (Yeager and Large, 2004). Such regions are found in the eastern subtropics of the North and South Pacific. As a passive tracer, spiciness anomalies are then advected adiabatically by the slow subsurface flow westward and towards the equator. The Argo data clearly shows these characteristics of spiciness generation and propagation after separating the spiciness signal from the temperature anomalies.

Figure 2.1 shows the propagation of spiciness anomalies in the Pacific from 2005 to 2012. Note that the depth integration is a better indicator of location of the anomalies rather than the peak intensity, since the spiciness anomalies may be localized on a narrow band of isopycnals. However, the depth integration may obscure a spiciness signal if opposite signed anomalies exist at the same location on separate isopycnals and cancel each other in the vertical integration. Figure 2.2 shows a depth versus time diagram that shows the intensity and depth of the anomalies clearly. A cool-fresh anomaly of around -0.3°C can be seen propagating to the southwest from 2005 to 2009 before diminishing in strength as it approaches the Mindanao Current at the western boundary. This anomaly was previously identified and studied by Sasaki et al. (2010) using salinity anomalies on isopycnal surfaces from Argo data. They showed that this anomaly subducted in 2004 between the 25σ and 25.5σ isopycnals and propagated towards the warm pool along isopleths of the mean Montgomery potential. In 2008, the last year of their data set, the anomaly was located near 10N and 160E which agrees with the data shown here. Their data also shows a strong warm-salty anomaly propagating toward the western boundary downstream of the cool-fresh anomaly that was the focus of their study. In the years since their research, another warm-salty anomaly has followed the cool-fresh anomaly indicating a possibly cyclic behavior to the generation of spiciness in the eastern subtropical North Pacific.

From 2005 to 2007, a warm-salty anomaly grows between 30°N-40°N and 120°W-140°W and reaches a peak of 1°C (Figure 2.2). Kilpatrick, Schneider and Di Lorenzo (2011) showed that anomalous geostrophic advection in the thermocline of this same region can generate low-frequency spiciness anomalies. Following the peak in growth, the anomaly propagates southwest with a speed of approximately 4.8 cm/sec (Figure 2.3), close to the subsurface geostrophic velocity as expected for a passive tracer. The strength of the anomaly dissipates as it progresses toward the western boundary, while the spatial extent grows, suggesting along-isopycnal diffusion as the cause of weakening signal strength. In addition, Figure 2.2 shows the time evolution of the signal at its generation

region and two locations downstream. The anomaly is shown to initially have its maximum between 25σ and 25.5σ in 2007 but in 2010 the maximum is between 24.5σ and 25σ. After 2011, the spatial extent of the anomaly extends south of 10°N in the interior basin indicating that some of the anomaly may have taken the interior pathway to the equator. However, the signal from the subtropics cannot be distinguished from locally generated anomalies in the tropical region (Schneider, 2000). As the anomaly reaches the western boundary at 10°N its magnitude has decreased significantly, but its spatial extent has spread longitudinally from the western boundary pathway across to the eastern boundary of the interior pathway in the central Pacific.

Another interesting aspect of the propagation is the local intensification of the anomaly once it reaches the equatorial western Pacific. A tongue of subsurface salty water from the South Pacific is known to frequently penetrate into the northern latitudes here, creating a subsurface salinity front that could generate spiciness anomalies if thermal anomalies are co-located in time and space, or via anomalous advection in the thermocline (Kilpatrick et al., 2011). One might speculate that the amplification may be due to the combination of spiciness anomalies of the same sign combining to amplify their signal.

In the South Pacific, spiciness anomalies are also shown to advect toward the equator within the pycnocline. Figure 2.1 shows an expansive cool-fresh anomaly from 2005 to 2006 with a depth average of -0.3°C in the eastern subtropical region where spiciness generation on subsurface isopycnals is known to be strong (Yeager and Large, 2007; Johnson, 2006). Figure 2.4a shows that the peak intensity of the anomaly is approximately -0.8°C and is located between the 25σ and 25.5σ isopycnals. With the large longitudinal span of the anomaly it would be expected that the eastern portion would follow the direct interior path toward the equator while the western portion would arrive at the equator further west. By 2008, the depth integrated anomaly seems to have diminished in spatial extent. However, this is due at least in part to anomalies of opposite sign offsetting each other in the vertical integration. In the 2008 panel of Figure 2.1, there is no anomaly in the region bounded by dashed lines. However, a Hovmüller diagram in this region (Figure 2.4b) shows that the anomaly is still present, although weaker, between the 25σ and 25.5σ isopycnals in 2008 but is offset in the depth integration by an anomaly of the opposite sign on a deeper isopycnal. A similar situation is found in 2009 when a portion of the anomaly approaches the equator from the interior pathway. Figure 2.4c shows an anomaly of the same sign, density, and amplitude passing through the region from 160W to 140W and 5S to 10S. This anomaly does not show up in the yearly mean depth integration because it is weak and it exists only partially in 2008 and 2009, but yet it is shown to pass through this region on its way to the equator. Furthermore, a Hovmüller diagram further

west and closer to the equator shows the same anomaly reached the dateline near the equator in 2010 (Figure 2.4d). The time between spiciness generation in early 2005 and the arrival of the spiciness anomaly at the equator is in agreement with the analysis of subtropical communication pathways of Wang and Huang (2005).

2.3 Temperature gradients across the pycnocline

As spiciness anomalies from each hemisphere converge in the western equatorial Pacific, they can alter the temperature gradient across the pycnocline. The extent to which this occurs is dependent on the strength and sign of the anomaly as well as on which isopycnal they are propagating. Figure 2.5 shows the temperature at given density values of all vertically interpolated Argo profiles within the EUC formation region of 160°E to the dateline within 3°of the equator from 2005-2013. Separating the the northern and southern data shows the character of the waters in each section. This assumes the water in the northern (southern) section is from the North (South) Pacific, i.e. the subsurface source waters do not cross the equator. This assumption is supported by the trajectory analysis of EUC source waters of Goodman et al (2005, their figure 10b). On a given isopycnal, the southern hemisphere waters tend to be warmer than the northern hemisphere waters within the pycnocline, taken here to be between 24σ and 26σ which is approximately the isopycnal range that wraps the EUC in this region (Gouriou and Toole, 1993). A subsurface high salinity tongue originating in the south Pacific does penetrate into the North Pacific in this region on these isopycnals in the time mean (Gouriou and Toole, 1993), but salinity anomalies within the salinity tongue would indicate the presence of spiciness just the same. In each hemispheric region, a range of 1-2°C exists on each isopycnal indicating a range of possible spiciness anomalies in the EUC formation region.

Plotting the slope of a linear regression of the temperature and density data for each year yields a time series of the temperature gradient across the pycnocline, or $\partial T/\partial \rho$ (Figure 2.6). The variability in the eight-year time series is around 10% peak to peak for each hemispheric region. Given the short duration of the time series it is likely that this variability is weaker than what would be seen in a longer time series. In addition, the large coherent spiciness anomaly shown to propagate mostly intact towards the western equatorial Pacific is stronger than its counterpart in the South Pacific, yet large amplitude spiciness anomalies are known to be generated there and propagate to the same region (Yeager and Large, 2007; Johnson, 2006). The nature of western equatorial Pacific as a crossroads of water masses (Fine, Lukas, Bingham, Warner and Gammon, 1994) would also suggest that low-frequency spiciness anomalies would induce variability at decadal timescales. If

the generation of these anomalies in the eastern subtropical North and South Pacific are the result of stochastic forcing and are independent of equatorial processes, then it is conceivable that large spiciness anomalies from both hemispheres could meet on the equator and bath the region in spiciness. Could this spiciness heat content have an effect on ENSO? If so, how would it alter its character? To explore this hypothesis, the next chapter will use insight from Figure 2.6 as input to the MZC model. The changes in $\partial T/\partial \rho$ seen in the Argo data will be used as a baseline for $\partial T/\partial \rho$ variability in the eastern equatorial Pacific cold tongue. In transit to the cold tongue region, $\partial T/\partial \rho$ would be modulated in the EUC due to along-isopycnal mixing with spiciness anomalies entering the EUC from an interior pathway in addition to diapycnal mixing. Turbulent entrainment with surface layers would also tend to weaken spiciness anomalies in the upper EUC. Nevertheless, the 10% variability shown here will be taken as a baseline for the variability within the EUC, and further amplification of this variability will simulate the possibility of spiciness anomalies converging on the equator.

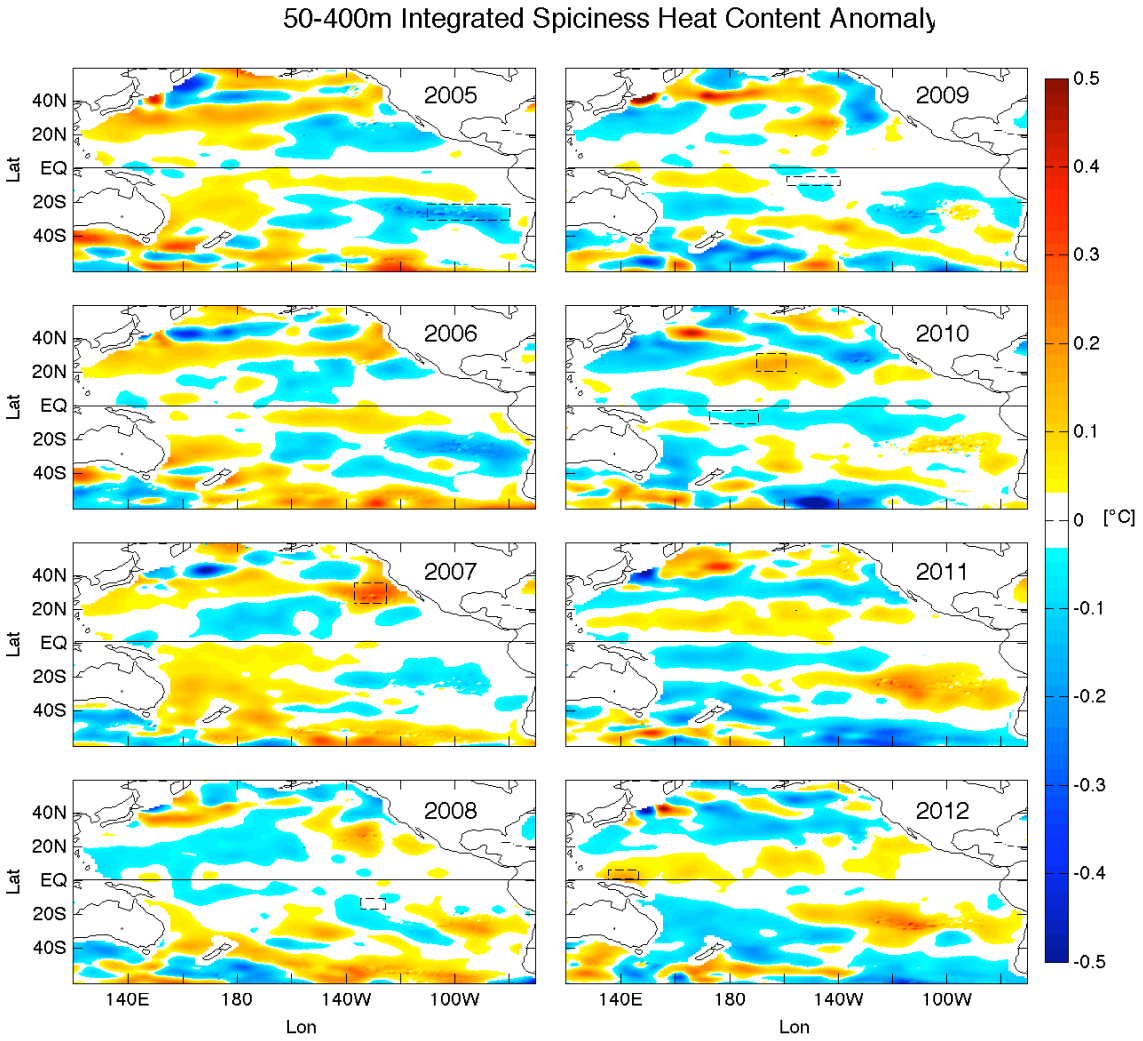

Figure 2.1. Depth integrated spiciness anomalies in the Pacific. The integration is performed from 50m to 400m using the trapezoidal rule. The top 50m are excluded to avoid surface processes in the mixed layer which could obscure the signal in the subsurface layers. Regions enclosed by dashed lines indicate the regions of the Hovmüller diagrams of Figure 2.2 and Figure 2.4. Anomalies less than 0.025 are white for clarity.

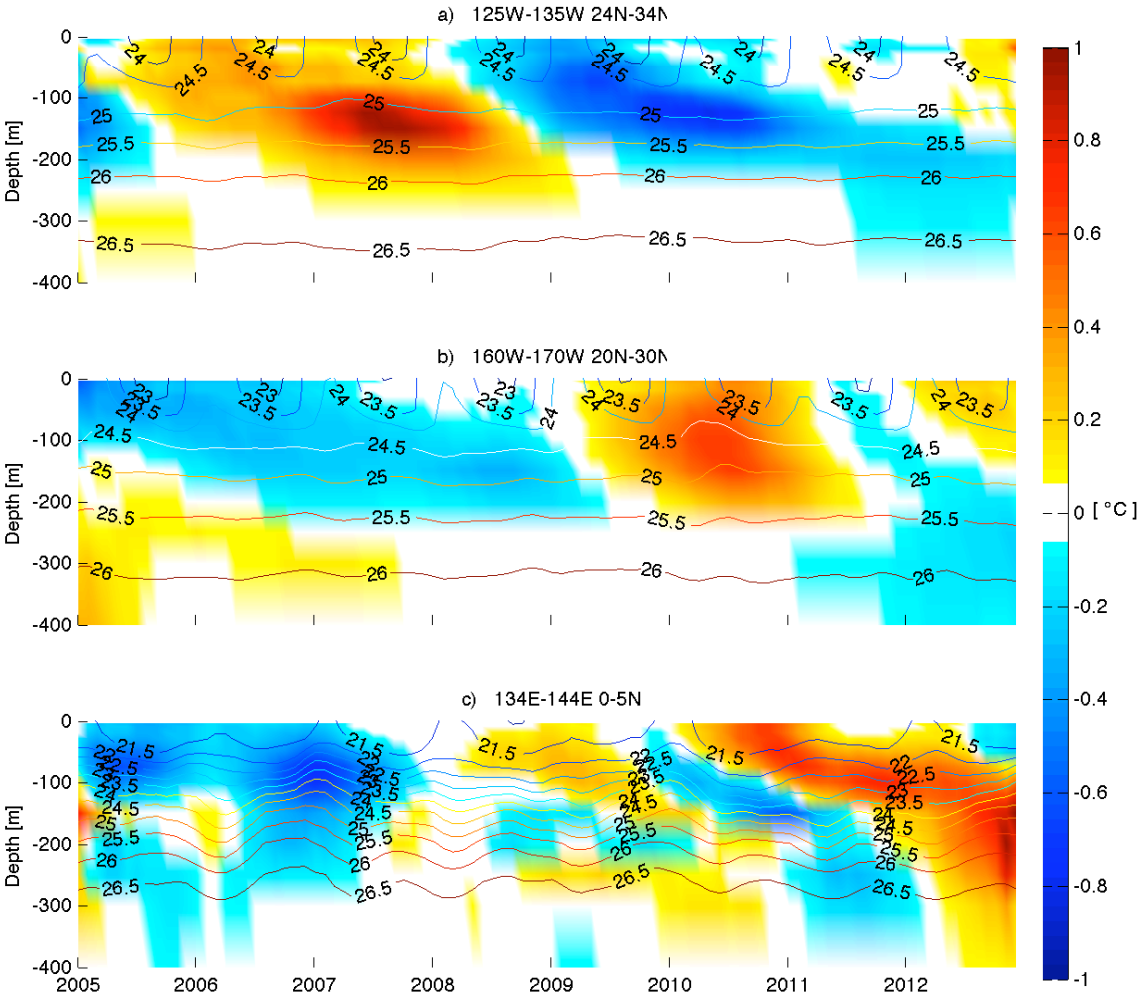

Figure 2.2. Hovmüller diagrams of North Pacific upper ocean spiciness anomalies in a) the generation region of the large positive anomaly in 2007 in Figure 1, b) the downstream location of the same anomaly in 2010, and c) the downstream location in 2012. Spiciness is smoothed by a 12-month running mean while isopycnals are smoothed by a 3-month running mean to capture the seasonality of outcroppings. Anomalies less than 0.05 C are white for clarity.

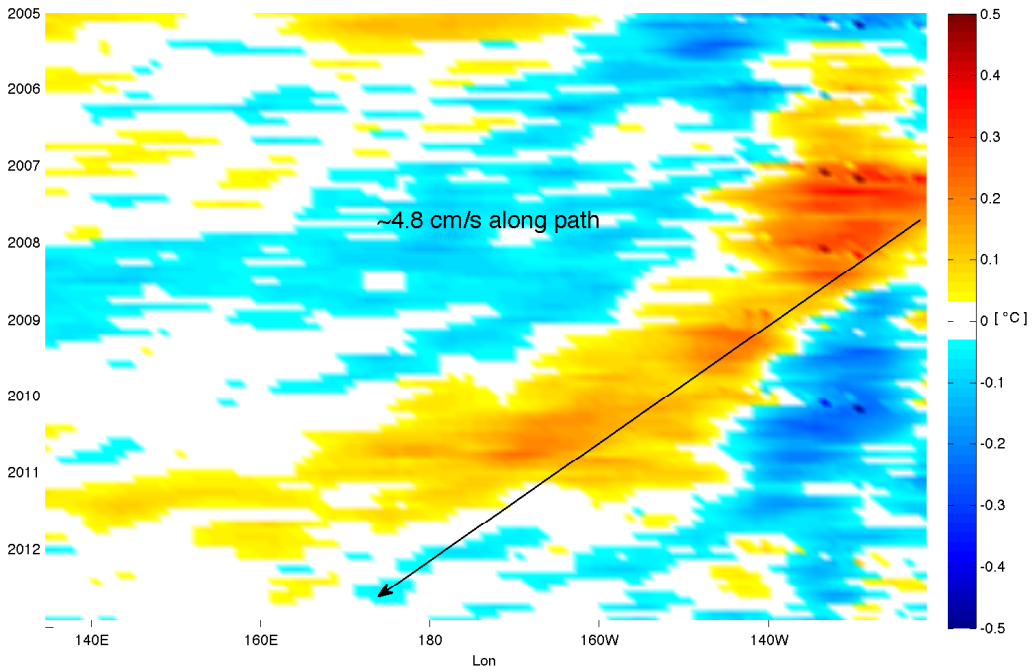

Figure 2.3. Hovmüller diagram of depth integrated spiciness heat content averaged over a diagonally oriented box along the advection path of North Pacific spiciness anomalies. The box extends from 10-20N, 135E to 25-35N, 120W. Anomalies less than 0.025 are white for clarity.

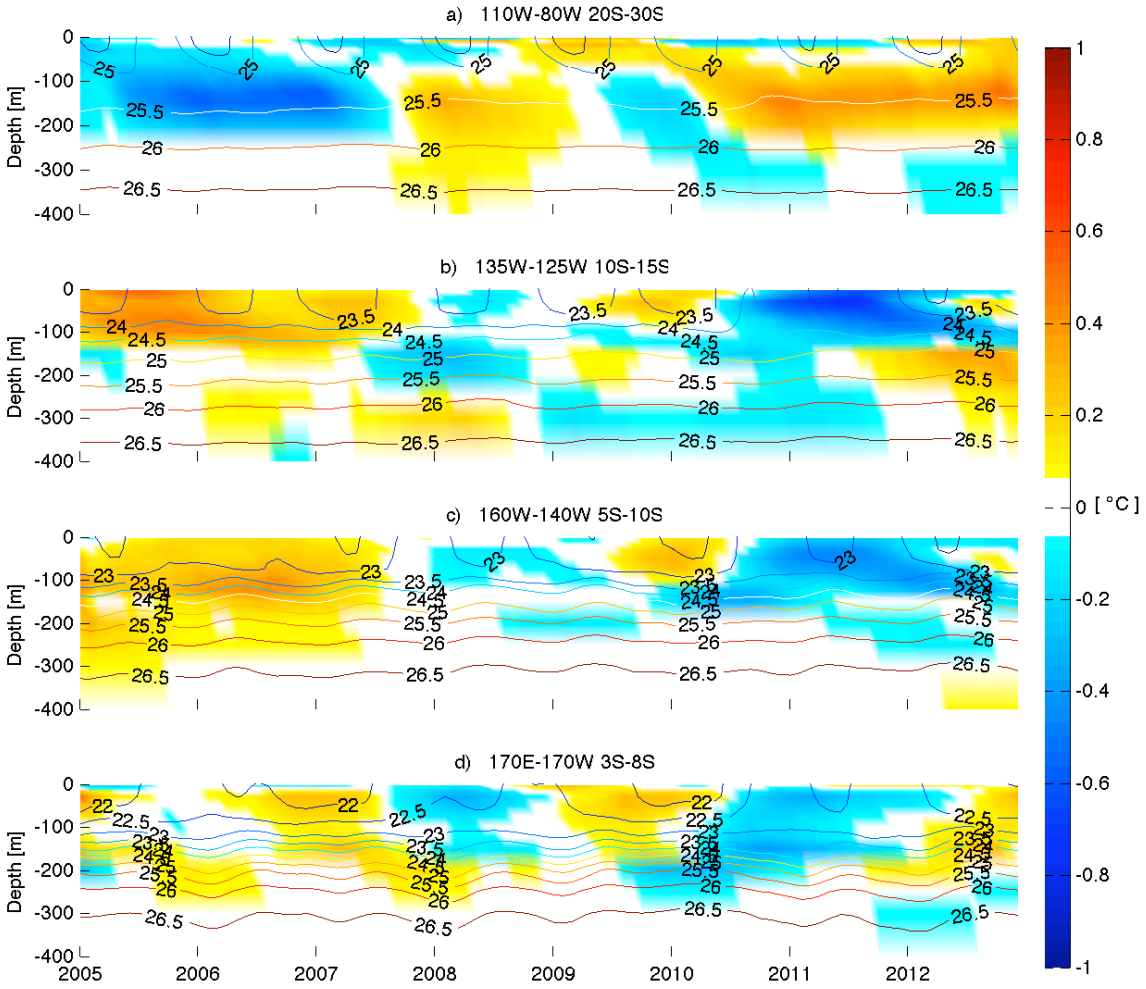

Figure 2.4. Same as Figure 2.2 except for the South Pacific. Plot a) is the generation region, b) is the downstream location of the interior path, c) is approximately the midpoint of the western boundary path, and d) is the downstream location as the anomaly approaches the equator.

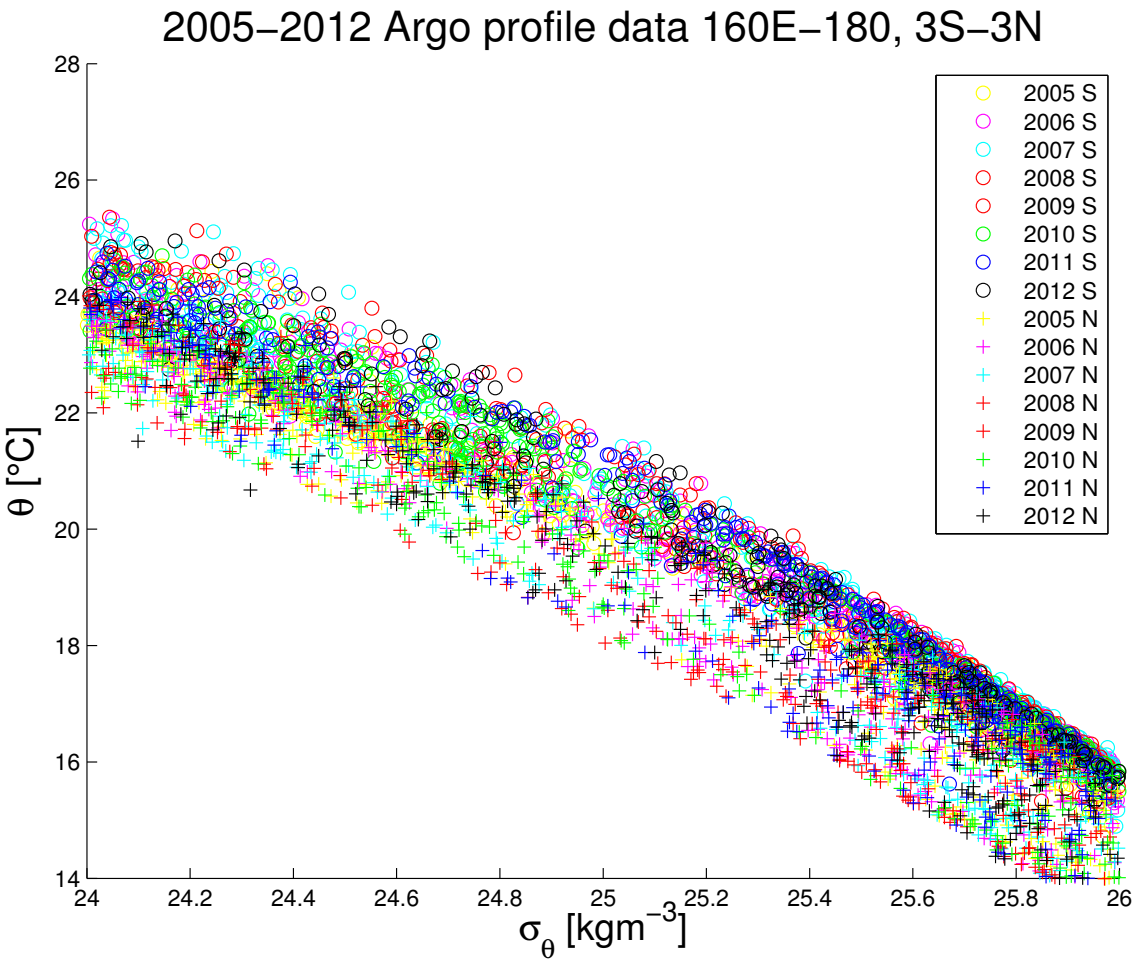

Figure 2.5. Potential temperature and potential density data in the EUC from all Argo vertical profiles between 160E and 180 and 3S to 3N from January 1, 2005 to December 31, 2012.

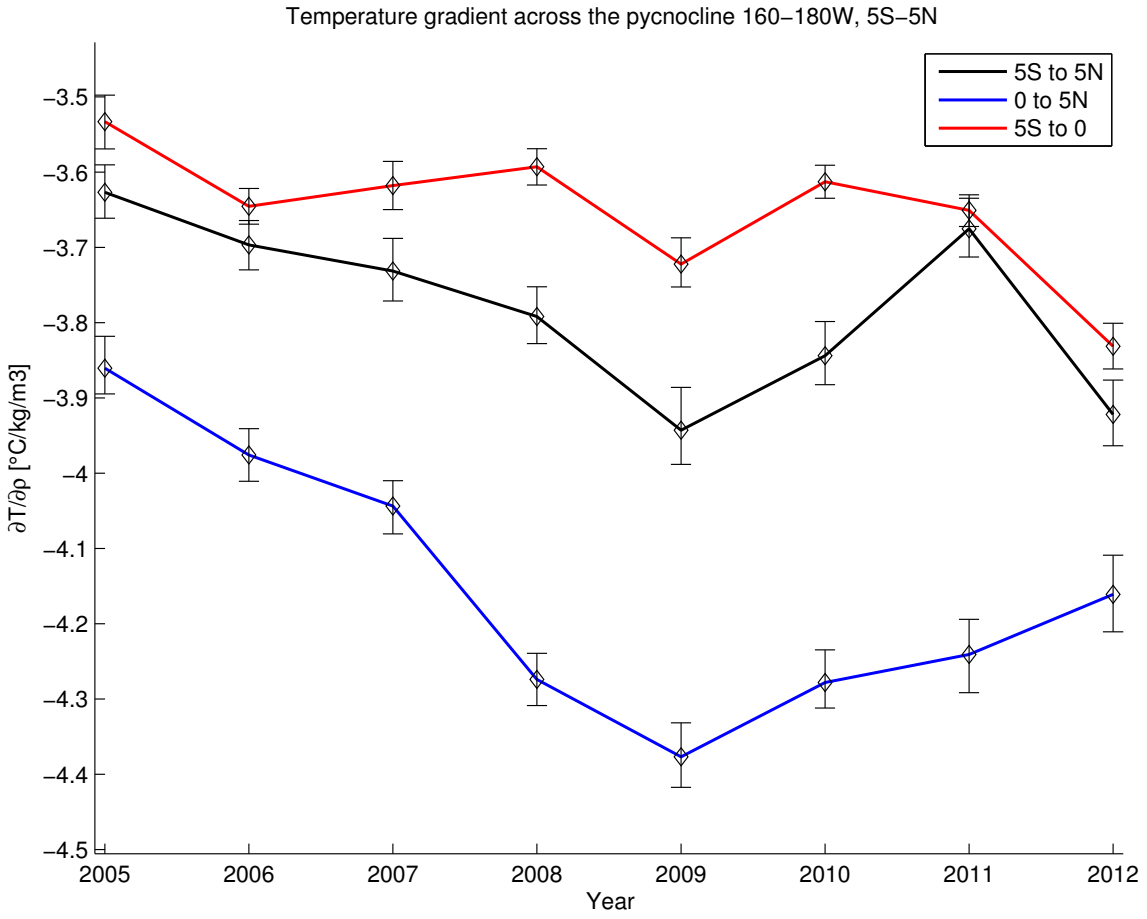

Figure 2.6. Times series of in the EUC formation region obtained by linear regression of potential density onto potential temperature for each year in the same region and using the same data as Figure 5. The regression is performed for all the data in the region and for the northern and southern portions separately as indicated in the legend. 95% confidence intervals are from a bootstrap estimation procedure.

Chapter 3

A modified Zebiak-Cane model of the El-Niño - Southern Oscillation

3.1 Model Description

In this chapter I use a version of the intermediate coupled model of the El Niño Southern Oscillation developed by Zebiak and Cane (1987) and modified by An and Wang (2000) and Bejarano and Jin (2008). The model is of intermediate complexity and reproduces the general characteristics of ENSO. Despite the prevalence of more advanced coupled models, the advantage of this model is that it allows for the exploration of the processes involved in ENSO without large computational expense. This allows variations to the model code to be executed quickly which facilitates exploration of the modeled ENSO.

The atmospheric component differs from the original ZC formulation and follows that of An and Wang (2000). It is an empirical model describing the linear relationship between observed SST and wind stress anomalies determined by singular value decomposition. The ocean component is a linear, reduced-gravity, shallow-water model on an equatorial beta plane and uses a long wave approximation (high-frequency, short-wavelength motions are excluded). The ocean basin in the model is rectangular and extends from 124°E to 80°W and 30°N to 30°S. The coupling is provided by a fixed-depth surface layer that is embedded in the upper active ocean layer. The wind stress from the model acts on the surface layer to simulate the wind-driven circulation. The model calculates anomalies relative to a prescribed full annual cycle in surface winds, surface wind divergence, SST, upwelling, and horizontal currents. The time step is set at 10 days.

The evolution of SST is controlled by the linear surface heat budget equation which has the form

$$\frac{\partial T}{\partial t} = -u\frac{\partial \overline{T}}{\partial x} - \overline{u}\frac{\partial T}{\partial x} - v\frac{\partial \overline{T}}{\partial y} - \overline{v}\frac{\partial T}{\partial y} - w_s\frac{\partial \overline{T}}{\partial z} - \gamma\overline{w}\frac{T - T_s}{H_1} - \alpha_s T \tag{3.1.1}$$

The overbar represents a climatological monthly mean and quantities without an overbar are anomalies. The first (second) term is the advection of the mean (anomalous) zonal temperature gradient by the anomalous (mean) zonal current. Similarly, the third (fourth) term is the advection of the mean (anomalous) meridional temperature gradient by the anomalous (mean) meridional current. The fifth (sixth) term is the advection of the mean (anomalous) vertical temperature gradient by the anomalous (mean) upwelling. The gamma represents an efficiency factor that accounts for the mixing of surface and subsurface waters at the base of the mixed layer, T_s represents the subsurface temperature, and H_1 is the upper layer thickness. The last term is the thermal damping of SST. Equivalently, the damping part of the advection of the anomalous vertical temperature gradient by the mean upwelling can be combined with the thermal damping term to isolate the positive feedback mechanism known as the thermocline feedback. The heat budget equation then becomes

$$\frac{\partial T}{\partial t} = -u\frac{\partial \overline{T}}{\partial x} - \overline{u}\frac{\partial T}{\partial x} - v\frac{\partial \overline{T}}{\partial y} - \overline{v}\frac{\partial T}{\partial y} - w_s\frac{\partial \overline{T}}{\partial z} + \gamma\overline{w}\frac{T_s}{H_1} - \left(\alpha_s + \frac{\gamma\overline{w}}{H_1}\right)T. \tag{3.1.2}$$

Although the ocean model is largely the same formulation as ZC, it has been modified in several ways from the ZC formulation. Details of four of these changes can be found in Bejarano and Jin (2008) but are summarized here:

1. The dynamic fields are expanded in Hermite polynomials according to Battisti (1988) in order to reduce the degrees of freedom.

2. The zonal resolution of the wave equations is reduced to reduce the degrees of freedom further.

3. To compensate for the numerical damping generated by 1) and 2) above, the weak linear damping in the oceanic momentum and continuity equations is set to zero.

4. The Heaviside function used in the ZC formulation to ensure downwelling doesn't affect SST is replaced with a hyperbolic tangent function.

The subsurface temperature function is also different and is parameterized as the displacement of a scaled time-mean vertical temperature profile. The function has the form

$$T_s = A * \left(\tanh\left(\frac{h - h_0}{B}\right) - \tanh\left(\frac{-h_0}{B}\right)\right) \tag{3.1.3}$$

where A is a scaler with units of temperature, h is the upper layer depth anomaly, h_0 = 15m, and B = 35m. This formulation differs from the ZC formulation in that the value of A varies with longitude and h_0 is constant and set to a shallow value. The magnitude of subsurface temperature anomalies is largely controlled by the values of A which determine the saturation limits of the hyperbolic tangent function. By design, the functional form resembles a time mean vertical temperature profile in the eastern Pacific. However, toward the western side of the basin the profiles resemble time mean profiles less and less as the saturation limits are scaled down. This simulates the stronger subsurface temperature anomalies at the base of the mixed layer in the eastern Pacific as the pycnocline ventilates, and the weaker subsurface temperature anomalies in the western Pacific where pycnocline ventilation does not occur. The profiles for the standard case are shown in Figure 3.4a.

In addition to these changes, the experiments performed here use three additional modifications to the model. First, since the primary concept that will be studied is the effect of spiciness in the pycnocline on ENSO, the T_s function should stay within the linear portion of the hyperbolic tangent function as much as possible. This means that upper layer depth anomalies should be modest and that model should stay as close to a linearly damped regime as possible. To this end, the behavior of the model as the strength of the coupling coefficient, μ, varies was analyzed to determine where the linearly damped regime exists in parameter space. The coupling coefficient controls the extent to which the winds drive the ocean dynamics through the parameterization of wind stress τ, which follows the standard bulk formula

$$\tau = \mu(\rho_0 C_d |\overrightarrow{u}|\overrightarrow{u}) \tag{3.1.4}$$

where C_d is the drag coefficient, ρ_0 is the reference air density, and $\overrightarrow{u}$ is the wind velocity. The values for reference air density and drag coefficient are the same as in the original ZC model. The model was run for 200,000 years with μ slowly increasing from 0.8 to 1.8. Figure 3.1 shows a plot of January SSTA versus μ shows the amplitude of ENSO as coupling is increased. Oscillatory unstable ENSO regimes do not appear until μ reaches values greater than 1.22. The coupling should not be too weak, however, and so a value of 1.10 is then chosen for μ.

In the linearly damped regime, the coupling between the atmosphere and ocean is too weak to generate the ENSO cycle. To obtain the ENSO oscillation, a Gaussian stochastic white noise forcing term is added to the zonal wind stress term in the central basin at each time step. The spatial mask used to apply the stochastic forcing is Gaussian in both the zonal and meridional directions and is centered on the equator at 170°W (Figure 3.2a). The ideal spatial pattern of stochastic wind stress forcing, or stochastic optimal, has a similar structure in the zonal winds, with convergence in the

eastern central basin (Moore and Kleeman, 1999). In this manner, the low-frequency portion of the white spectrum will excite eastward propagating equatorial Kelvin waves and westward propagating Rossby waves similar to a westerly wind burst while the high-frequency noise will be filtered out by the ocean dynamics.

To determine the appropriate amount of stochastic forcing to add to the model, a series of 500-year model runs were performed with μ set to 1.10 and the stochastic noise scaled by various constant values. Wind stress attributed to SST accounts for 29% of wind stress variance, while the remaining 71% of the variance can be attributed to random atmospheric variability (Syu, Neelin and Gutzler, 1995; Blanke and Raynaud, 1997). Since the statistical atmospheric model used here determines wind stress anomalies from a prescribed SST, the ratio of variance of the wind stress due to the applied stochastic forcing to the total variance of the wind stress should be near 0.71. Trials were performed with scale factors ranging from zero to one to find a scale factor that gives a ratio near 0.71 at the center of the mask where the forcing is greatest. The results are shown in Figure 3.2b. Also plotted is the standard deviation of NINO3 SSTA to determine ENSO amplitude with increasing scale factor. With a weak scale factor of 0.1 the desired ratio is nearly met, but this is due to weak ENSO amplitude, weak SST anomalies, and therefore weak wind stress from the atmospheric model and a high ratio of stochastic wind stress. As ENSO amplitude increases to realistic values, the ratio decreases, then begins to increase again. A stochastic scale factor of 0.75 was chosen as it gives the ratio needed with a realistic ENSO amplitude.

All other aspects of the model remain the same as the ZC formulation. The full model equations and parameter values aside from the changes mentioned above can be found in the Appendix of Zebiak and Cane (1987), while the full description of changes made by Bejarano and Jin (2008) can be found in Bejarano (2006).

With the μ set to 1.10 and the stochastic forcing scale factor set to 0.75, the standard case model is set. Figure 3.3 shows the first 200 years of the NINO3 SSTA time series smoothed with a 12-month moving average and the spectrum of a 500 year simulation. The spectrum has most of its power between three and five years with its peak at four years. The El Niño events reach peak amplitudes of around 3°Celsius with La Niña reaching approximately -1°Celsius.

3.2 Introducing Spiciness to the Model

As low-frequency spiciness anomalies propagate in the pycnocline along the EUC to the eastern equatorial Pacific where they upwell into the mixed layer, the time mean vertical temperature

profile in the thermocline will be altered. The vertical temperature gradient can be decomposed into two components:

$$\frac{\partial T}{\partial z} = \frac{\partial T}{\partial \rho}\frac{\partial \rho}{\partial z} \tag{3.2.1}$$

The first component is the temperature gradient across the pycnocline as we have been using, and the other is the stratification. Since this model does not have a density structure, the thermocline and pycnocline are the same and changing the vertical temperature gradient in the thermocline, via the T_s function, simulates the effect of spiciness anomalies. The presence of a cool and fresh (warm and salty) spiciness anomaly in the upper (lower) pycnocline will weaken the vertical temperature gradient of the pycnocline, while a warm and salty (cool and fresh) anomaly in the upper (lower) pycnocline will strengthen it. This effect, however, is limited to isopycnals of the pycnocline and for this reason a linearly damped regime is chosen for the model to reduce the likelihood of upper layer depth anomalies causing the subsurface temperature function to reach saturation values. Figure 3.4b shows the profile at 95°W for the standard case and sample profiles in which spiciness anomalies are present.

To introduce a change in the slope of the T_s function, different values A and B will be used to alter its functional form. With T_1 representing the standard T_s function and T_2 representing the new function, the two equations can be written as

$$T_1 = A_1 * \left(\tanh\left(\frac{h-h_0}{B_1}\right) - \tanh\left(\frac{-h_0}{B_1}\right)\right) \tag{3.2.2}$$

$$T_2 = A_2 * \left(\tanh\left(\frac{h-h_0}{B_2}\right) - \tanh\left(\frac{-h_0}{B_2}\right)\right) \tag{3.2.3}$$

with A_1, B_1, and h_0 are known quantities. Care must be taken to ensure that only the slope is changed and not the saturation limits of the hyperbolic tangent function. This condition can be written for the upper limit as

$$A_1 * \left(1 - \tanh\left(\frac{-h_0}{B_1}\right)\right) = A_2 * \left(1 - \tanh\left(\frac{-h_0}{B_2}\right)\right) \tag{3.2.4}$$

and for the lower limit as

$$A_1 * \left(-1 - \tanh\left(\frac{-h_0}{B_1}\right)\right) = A_2 * \left(-1 - \tanh\left(\frac{-h_0}{B_2}\right)\right) \tag{3.2.5}$$

For these equalities to hold, different values for B are needed for the upper and lower halves of the T_2 function, which necessitates two individual functions for positive and negative h values. Solving

for the upper and lower values of A, now called A_{2U} and A_{2L}, we have

$$A_{2U} = A_1 * \frac{1 - \tanh\left(\frac{-h_0}{B_1}\right)}{1 - \tanh\left(\frac{-h_0}{B_{2U}}\right)} \tag{3.2.6}$$

$$A_{2L} = A_1 * \frac{-1 - \tanh\left(\frac{-h_0}{B_1}\right)}{-1 - \tanh\left(\frac{-h_0}{B_{2L}}\right)} \tag{3.2.7}$$

where B_{2U} and B_{2L} are the distinct values for the upper and lower function. In addition, it is desirable to have the first derivative be continuous at h=0, the center of the thermocline. This condition can be written as

$$\frac{\partial T_2}{\partial h} = \frac{A_{2U}}{B_{2U}} * \frac{1}{\cosh^2\left(\frac{-h_0}{B_{2U}}\right)} = \frac{A_{2L}}{B_{2L}} * \frac{1}{\cosh^2\left(\frac{-h_0}{B_{2L}}\right)} \tag{3.2.8}$$

These conditions ensure that the resulting profile is essentially unchanged from the original profile with the exception of the change in slope within the thermocline. For the four unknown values A_{2U}, A_{2L}, B_{2U}, and B_{2L} we have only three equations. Therefore, a desired change in slope is specified and incremental values for B_{2U} are used to calculate the resulting slopes. The B_{2U} value that minimizes the difference between the calculated slope and the specified slope is chosen. The same routine is applied to find the value of B_{2L}.

This method does have limitations. When attempting to increase the slope to a value above 10% of the initial value, the function takes on an unrealistic form. Decreasing the slope does not have this problem. Another limitation is that the addition of spiciness is stronger for positive upper layer depth anomalies for a given slope change. Both of these issues arise from the use of vertical and horizontal offsets in the hyperbolic tangent function, i.e. the function is not symmetric (see Figure 3.4). The reason for the asymmetry is to prevent excessive subsurface temperature anomalies after the thermocline has shoaled to the surface.

3.3 A 20,000 year model integration

To determine the effect of spiciness on ENSO period and amplitude a wavelet analysis is used. Wavelet software was provided by Torrence and Compo (1998), and is available at URL: `http://atoc.colorado.edu/research/wavelets/`. Wavelet analysis typically

has time as one of three axes, but in this experiment the slope of the T_s function is varied linearly with time, from a 70% reduction in slope to a 10% increase, and so the change in slope replaces the time axis. Using this technique, a change in both ENSO period and SSTA variance, if any, can be easily seen as spiciness is slowly varied in the NINO3 region. The model is run over 20,000 years so that low-frequency changes in spiciness can be simulated. The mother wavelet used was a Morlet wavelet with scales from 6 months to 64 years. Seven powers-of-two were used with 4 sub-octaves each. The resulting wavelet is shown in Figure 3.5.

The reference run corresponds to the horizontal axis value of 100%, with smaller ratios indicating weaker $\partial T/\partial \rho$ and larger ratios indicating stronger $\partial T/\partial \rho$. In the following discussion it is important to make the distinction between the vertical temperature gradient in the T_s function, or equivalently $\partial T/\partial \rho$, which represents the time-mean vertical temperature profile, and the anomalous vertical temperature gradient in the SSTA tendency equation, which is a function of the SST and the temperature anomaly from the T_s function (see equation 3.1.1). In this model, the time-mean vertical temperature profile is predetermined and its displacement is used to determine the anomalous subsurface temperature. Low-frequency spiciness anomalies will alter the mean state vertical temperature (and salinity) structure, which is reflected here by a change in $\partial T/\partial \rho$. A weakening of $\partial T/\partial \rho$ is equivalent to a cool-fresh spiciness anomaly in the upper pycnocline and a warm-salty anomaly in the lower pycnocline.

The results from this experiment indicate that as $\partial T/\partial \rho$ gets stronger (weaker), the variance of ENSO is increased (decreased), while the wavelet spectrum shows no change in the dominant period of ENSO. In terms of the model equations the explanation for the increase in variance is straightforward. The influence of the T_s function in the SST tendency equation is through the mean upwelling on the anomalous vertical temperature gradient. For weak $\partial T/\partial \rho$, as the upper layer depth anomaly increases (decreases) and the pycnocline deepens (shallows) during El Niño (La Niña), the cool-fresh (warm-salty) spiciness anomaly at the top (bottom) of the pycnocline reduces (increases) the temperature at the base of the mixed layer and strengthens (weakens) the anomalous vertical temperature gradient, damping the SSTA. The reverse scenario is true for stronger $\partial T/\partial \rho$. The spiciness anomalies that are exposed to the mixed layer enhance the SSTA and lead to stronger events, and more variance.

To understand this result more clearly, the change in the heat budget terms corresponding to the positive feedbacks of ENSO, collectively known as the Bjerknes feedback, are studied. The horizontal advection feedback is the advection of the climatological zonal SST gradient by the anomalous zonal current, the thermocline feedback is the advection of the anoma-

lous vertical temperature gradient by the climatological mean upwelling, and the Ekman feedback is the advection of the climatological vertical temperature gradient by the anomalous upwelling. Of the three primary positive feedbacks that amplify SST anomalies, the thermocline feedback and horizontal advection feedback are key mechanisms in the growth of ENSO (Battisti and Hirst, 1989; Jin, 1996; Jin, 1997*a*; Jin, 1997*b*; An and Jin, 2001), while the Ekman feedback plays a somewhat lesser role. However, in these model experiments the horizontal feedback term is quite small due to low amplitude anomalous currents resulting from the weak coupling coefficient used. This misrepresentation of the horizontal feedback term is a limitation of the model.

Figure 3.6 shows composites of the NINO3 SST anomaly and heat budget terms created from 35 ENSO cycles of 500-year model runs with $\partial T/\partial \rho$ at 70% and 110% of the standard run values. The NINO3 SSTA time series shows a difference of nearly 1°C between composited El Niño events and approximately 0.5°C between composited La Niña events, clearly showing how ENSO amplitude increases with increasing $\partial T/\partial \rho$. The mechanisms driving the response can be understood by looking at composites of the dominant terms: the thermocline feedback, the Ekman feedback, and the advection of the anomalous meridional temperature gradient by the mean meridional currents. Under weak $\partial T/\partial \rho$, the growth rate of these terms and the total SSTA is decreased. Under strong $\partial T/\partial \rho$ conditions, the terms show a stronger rate of growth and decay. This result is expected and is indicative of a stronger thermocline feedback term. As $\partial T/\partial \rho$ increases, the temperature change across the pycnocline becomes larger and the subsurface temperature parameterization becomes more like a step function and reaches its saturation limits with less displacement of the pycnocline. This gives more sensitivity to the thermocline feedback term and an increase in the SSTA growth rate. As $\partial T/\partial \rho$ becomes weaker, thermocline displacements would alter the anomalous subsurface temperature and thus the thermocline feedback term less.

The Ekman feedback is seen to grow stronger (weaker) with increasing (decreasing) $\partial T/\partial \rho$. This result is likely a passive result of increasing ENSO strength. The anomalous upwelling is a function of the divergence of the anomalous equatorial surface currents, which are themselves a function of the zonal winds. As the thermocline feedback works to bring stronger ENSO variance, the variance in zonal winds increases in concert bringing with it increased variance in equatorial upwelling. The growth of the Ekman feedback is likely an adjustment to the growth in the thermocline feedback.

Surprisingly, the term corresponding to the advection of the anomalous meridional temperature gradient by the mean meridional currents is the strongest term in this model. This is can be understood by taking into consideration the spatial extent of this term and the thermocline feedback

term in the NINO3 region. Equatorial upwelling is localized to around 2 degrees north and south of the equator and so the thermocline feedback can only contribute to NINO3 SSTA in this narrow strip on the equator. The mean meridional currents in the NINO3 region are always poleward and so the meridional advection feedback term depends primarily on the direction of the anomalous meridional temperature gradient, which changes sign with ENSO. As the thermocline feedback term creates localized SST anomalies on the equator in the NINO3 region, an anomalous meridional temperature gradient is set up that is then advected by the mean meridional currents. This meridional advection is more effective in filling the NINO3 region with anomalous SST than the thermocline feedback term that sets up the anomalous meridional gradient. During both El Niño and La Niña, this term is a positive feedback and contributes to the growth of each phase of ENSO. Like the Ekman feedback, the strength of this term adjusts itself with the strength of the thermocline feedback.

After looking at these three feedback mechanisms it is clearly seen that the positive feedback mechanisms of ENSO grow or weaken in concert with $\partial T/\partial \rho$, leading to increased ENSO variance. These results show that as spiciness enters the equatorial pycnocline and advects east to the cold tongue region, there is a possibility that they can have a significant effect on ENSO character. Of course, this depends on the magnitude of the anomalies and long residence time in the cold tongue region, but observations from Argo indicate that this possibility is not unrealistic. The increased variance is a result of the increased non-linearity in the coupled system. Specifically, the dominant non-linearity of the Zebiak-Cane model lies in the subsurface temperature parameterization, which is directly affected by changes in spiciness. Weak (strong) $\partial T/\partial \rho$ increases (decreases) the range of upper layer depth anomalies that result in a near linear response in subsurface temperature and decreases (increases) the likelihood of reaching the saturation limits of the hyperbolic tangent function. If the system were only weakly non-linear then the distribution of temperature values in the NINO3 time series would approximately be normal, and so deviations from a normal distribution in the NINO3 time series can be used to determine the extent of non-linearity (Burgers and Stephenson, 1999). Figure 3.8 shows distributions of SSTA in the NINO3 region for 500-year model runs with $\partial T/\partial \rho$ set at 70% and 110% as well as normal distributions with the same mean and standard deviation as the data. Under weak $\partial T/\partial \rho$ conditions, the distribution is nearly normal and displays only weakly positive skewness. However, under strong $\partial T/\partial \rho$ conditions the distribution deviates markedly from normality and becomes multimodal with extreme values becoming more likely. This is a consequence of changes in sensitivity of the thermocline feedback and non-linearity of the system as spiciness alters the time-mean vertical temperature profile.

Although ENSO variance within the model has been shown to change as a result of spiciness, the center of action of ENSO was not affected. To determine the extent of change in the location of ENSO SSTA maximum with strong or weak $\partial T/\partial \rho$, SST anomalies within five degrees of the equator were averaged for each zonal grid point to create an equatorial average SST anomaly for each time step of the 20,000 year experiment. A 500-year running standard deviation was then passed through the resulting time series for each zonal grid point. Figure 3.7 shows the resulting Hovmüller diagram. It shows clearly that the standard deviation of NINO3 SSTA increases with time only in the eastern equatorial Pacific and the center of action is unchanged. However, this result is only due to the model's inability to generate ENSO away from the NINO3 region. The subsurface temperature functions in the NINO4 region have their saturation limits severely limited (see Figure 3.4) and so even with large spiciness anomalies and large undulations of the thermocline the resulting subsurface temperature anomaly is very weak.

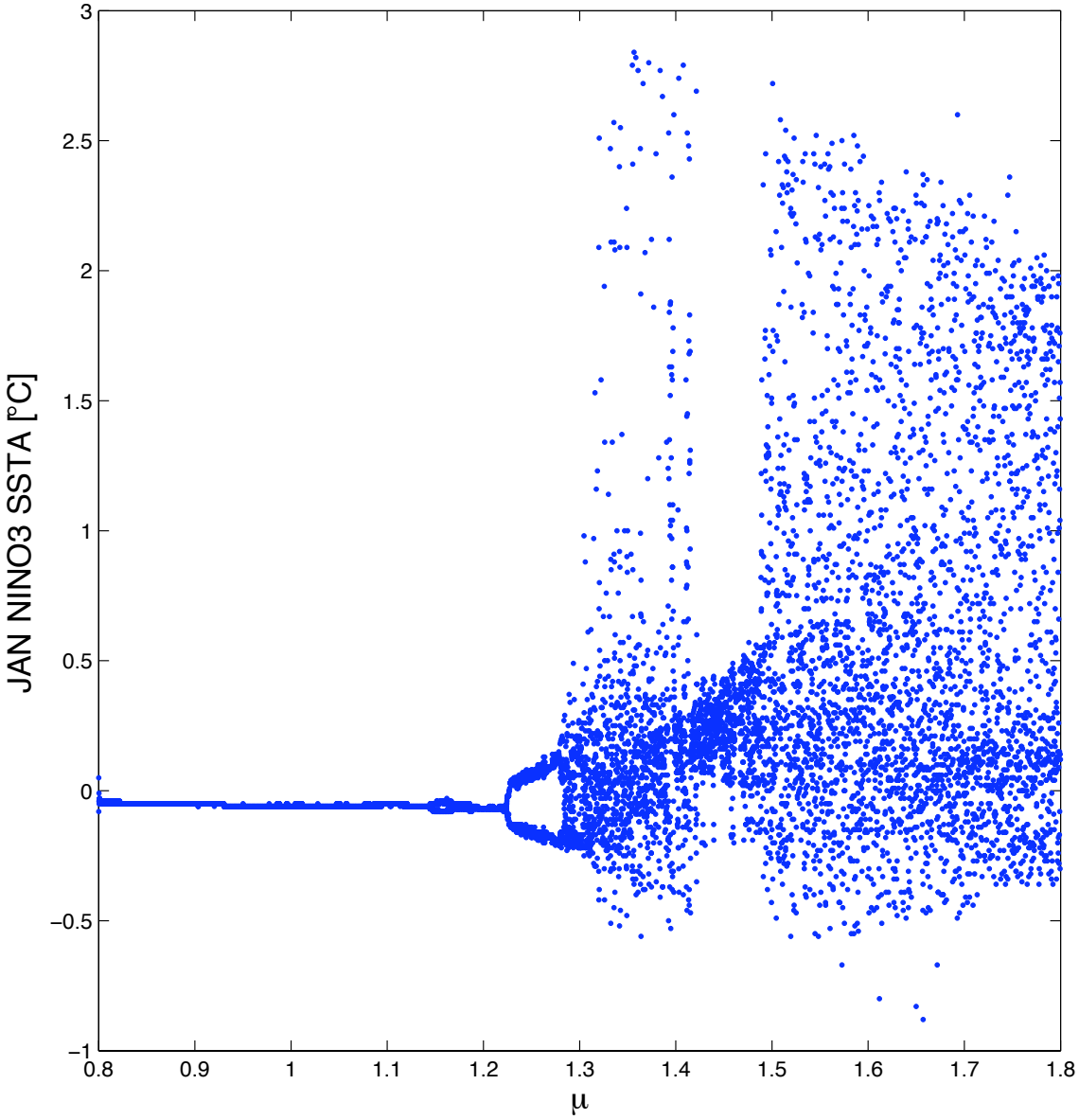

Figure 3.1. Bifurcation diagram of the modified ZC model with varying coupling coefficient, μ.

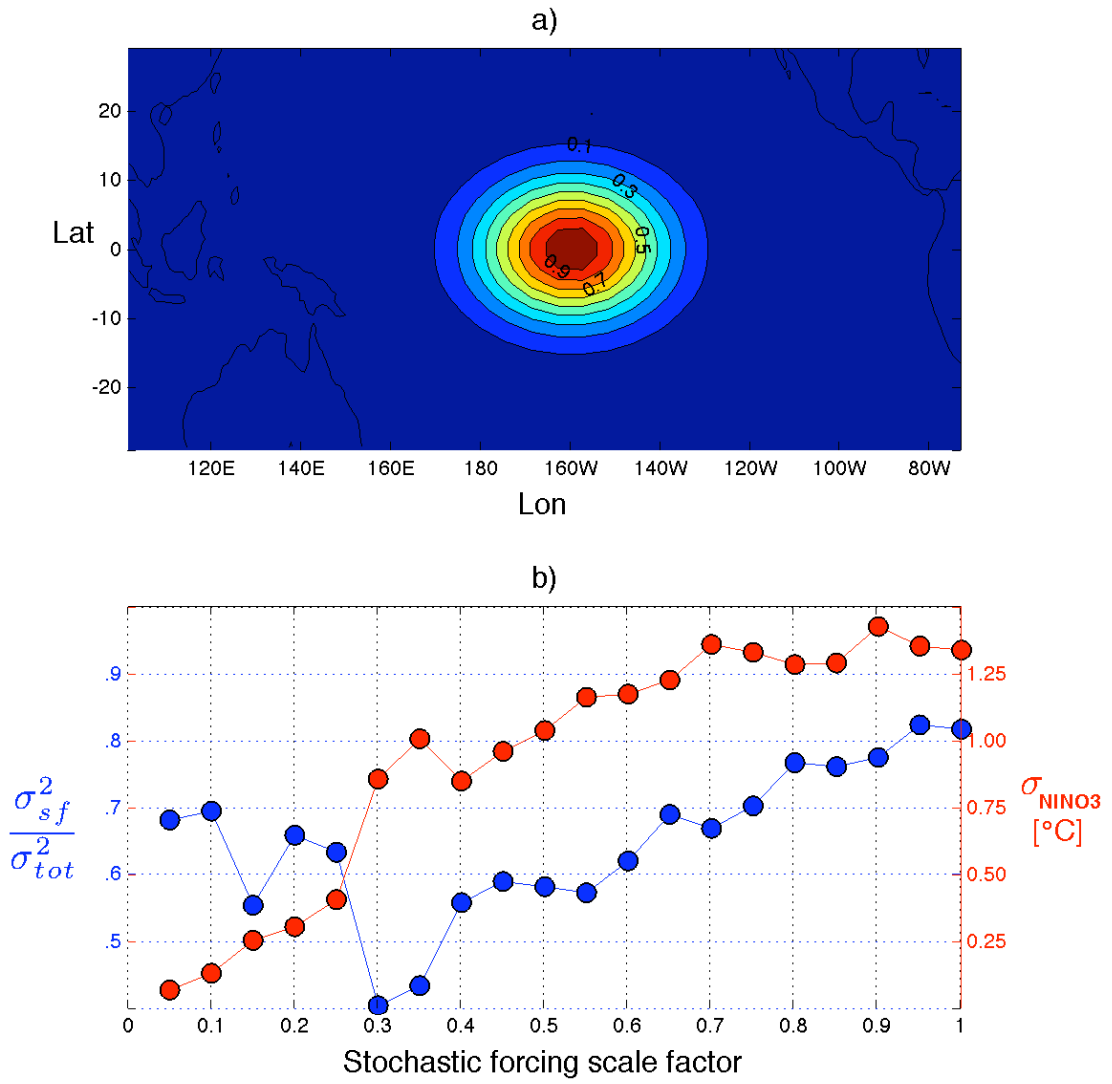

Figure 3.2. a) The stochastic forcing mask used to confine the forcing to the central Pacific, and b) the results from the stochastic forcing trials. The blue dots in b) show the fraction of zonal wind stress variance in the center of the mask due to stochastic forcing, while the red dots show the standard deviation of NINO3 SSTA during the same trial run. The land masses in a) are shown for reference only.

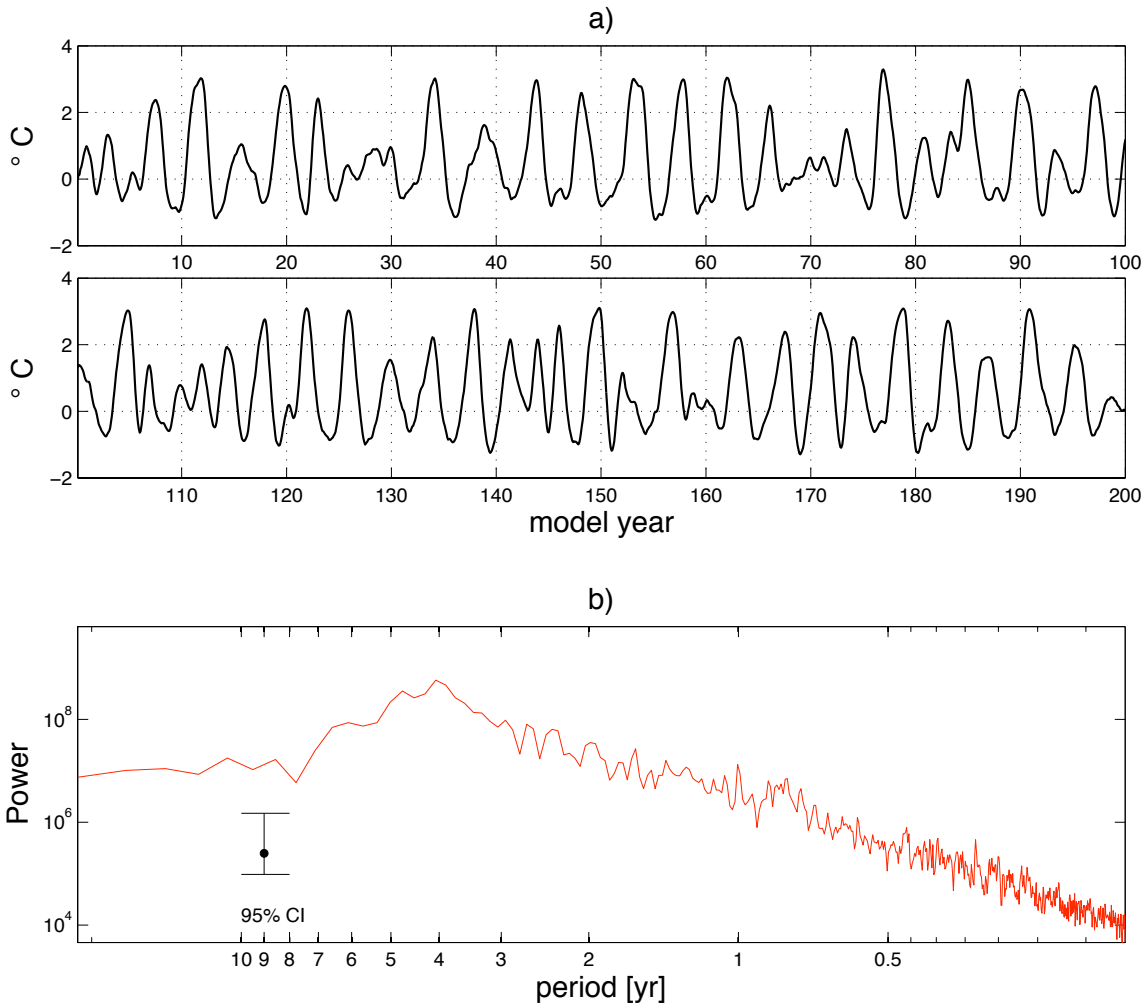

Figure 3.3. The first 200 years of a 500-year run of the standard model normalized NINO3 SSTA, and b) its spectrum.

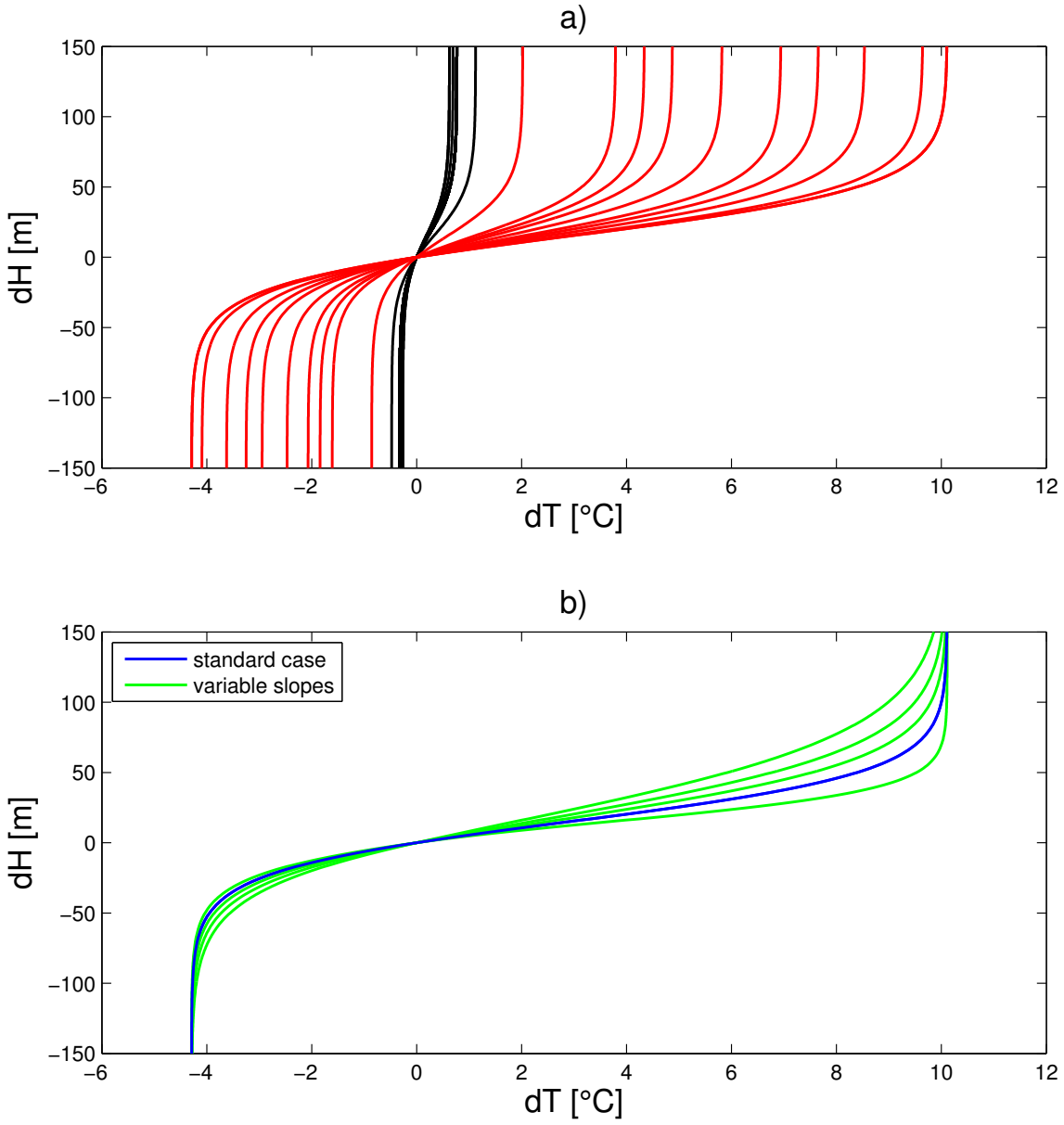

Figure 3.4. a) Profiles for the subsurface temperature parameterization. Profiles in red indicate the profiles in the NINO3 region and those in black are west of NINO3. The widths of the functions decrease monotonically to the west. b) Sample profile at 95W (blue) and modified versions of the same profile (green) using the technique developed in section 3.2 demonstrating the introduction of spiciness.

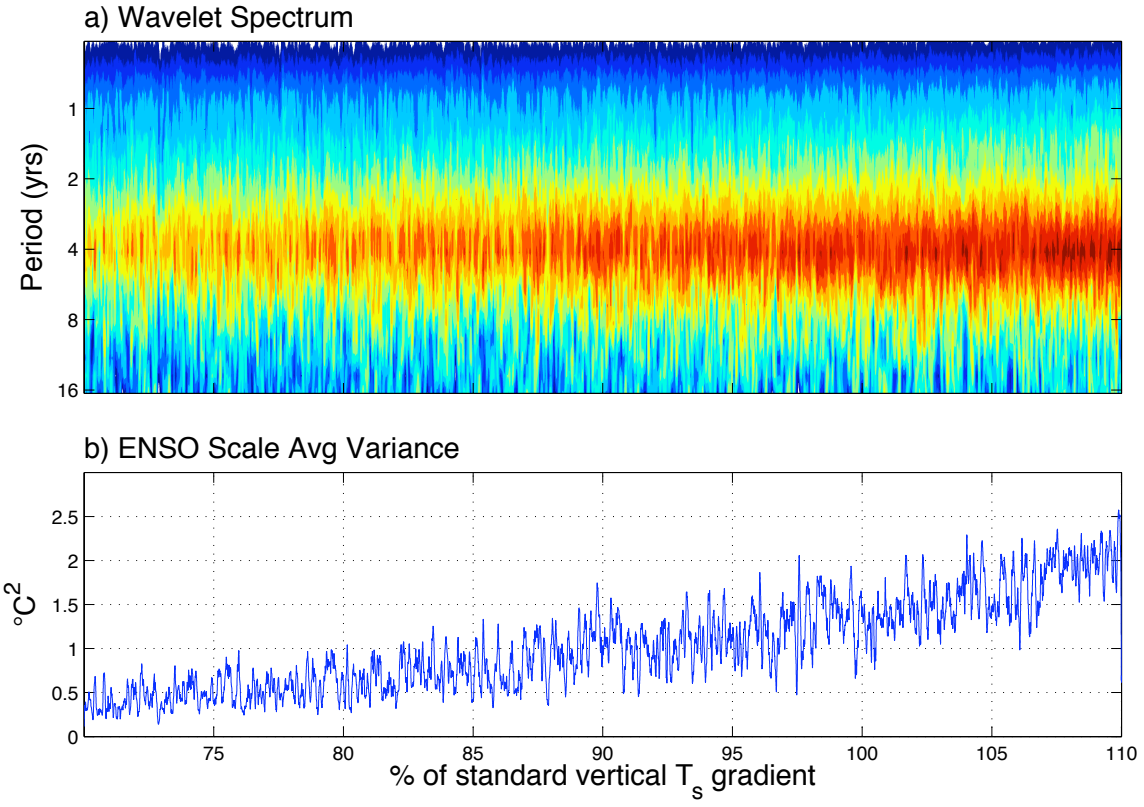

Figure 3.5. a) Wavelet spectrum for 20,000 year model integration with varying $\partial T/\partial \rho$. b) Variance of the 2-8 year scale average NINO3 time series.

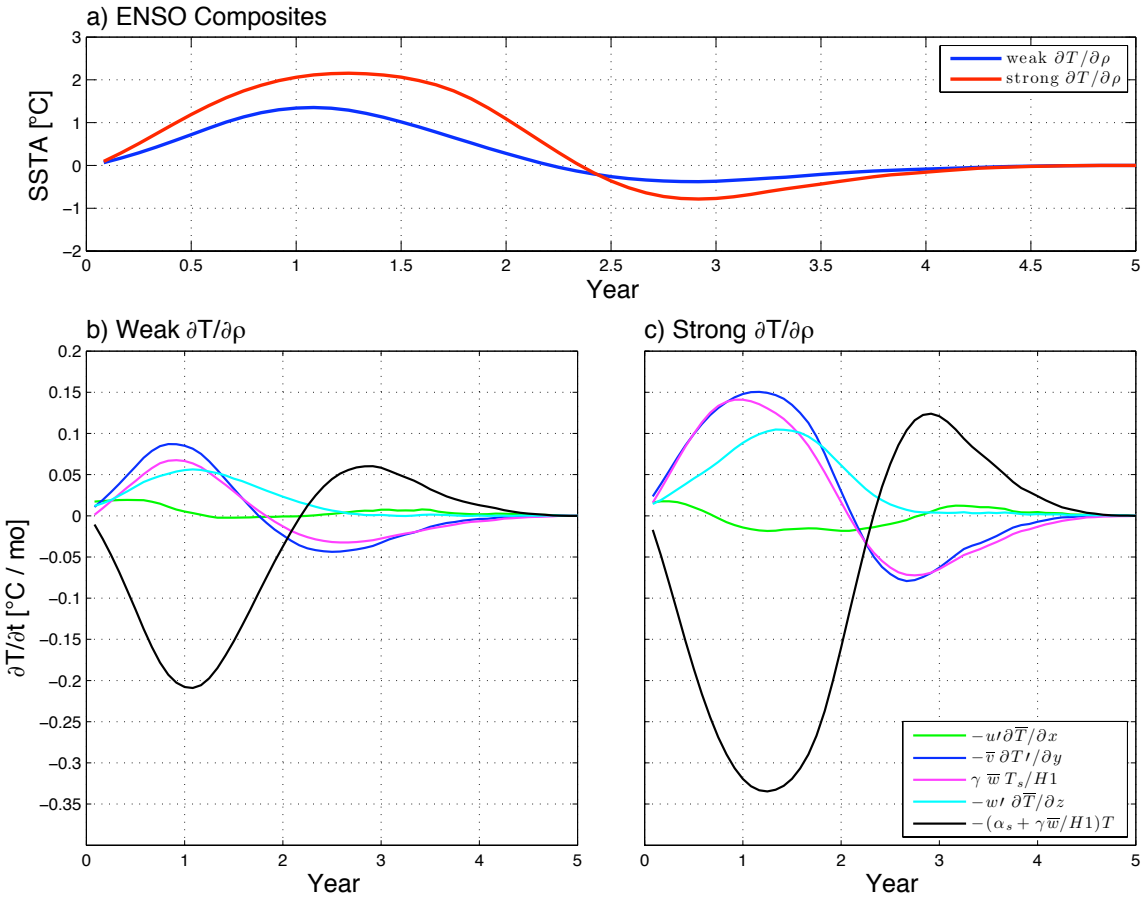

Figure 3.6. Composites of 35 ENSO events during 500 year model runs with $\partial T/\partial\rho$ at 70% and 110% of original value. a) NINO3 SSTA composites and b) and c) composites of the heat budget terms during weak and strong $\partial T/\partial\rho$, respectively.

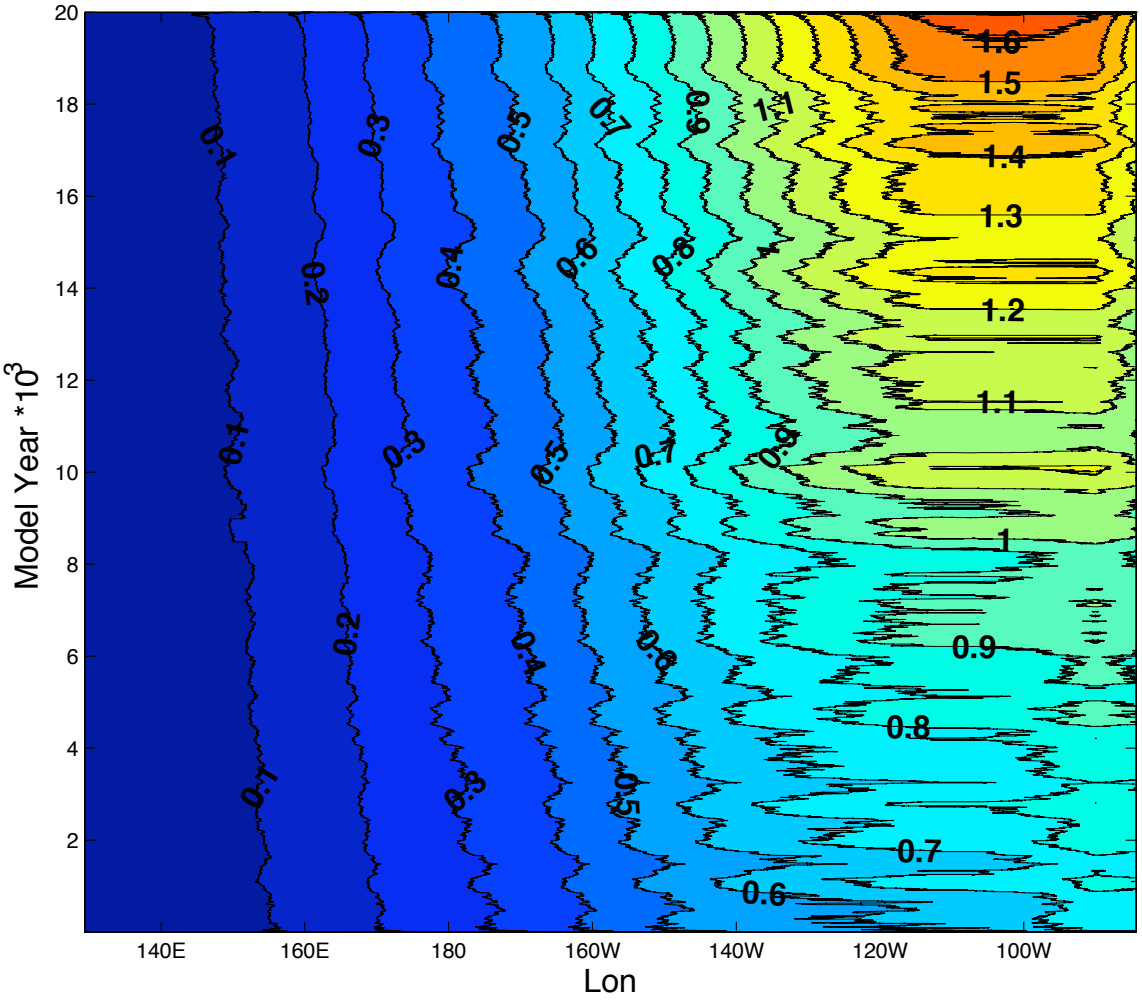

Figure 3.7. Hovmüller diagram of equatorial average SSTA standard deviation as a function of time and longitude. Contour labels are in °C.

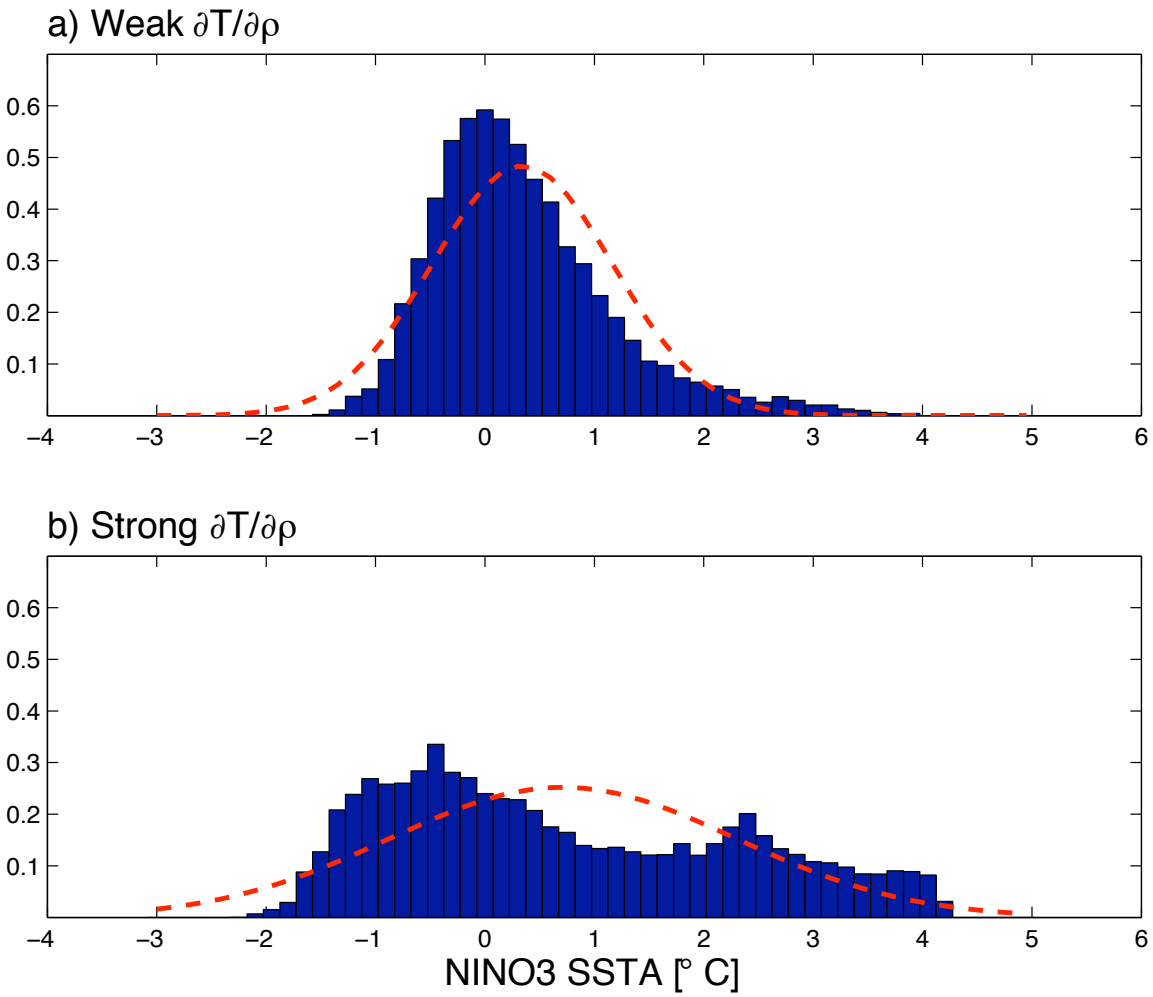

Figure 3.8. Distributions of NINO3 SSTA under weak and strong $\partial T/\partial \rho$ conditions. Red dashed lines are normal distributions with the same mean and standard deviation as the binned data. Bin widths are 0.15 degrees C.

Chapter 4

Summary and Conclusions

In this thesis the propagation of spiciness anomalies into the equatorial Pacific and their effect on ENSO was investigated. The Argo observational data clearly shows the generation and propagation of decadal spiciness anomalies from the subtropical to the tropical Pacific within the pycnocline. Spiciness anomalies alter the temperature gradient across the pycnocline, $\partial T/\partial \rho$, and in the western equatorial Pacific $\partial T/\partial \rho$ was shown to vary interannually by approximately 10% peak to peak over the short eight-year time series. Decadal variations of $\partial T/\partial \rho$ in the EUC are likely given the time it takes spiciness anomalies to propagate from their generation regions to the equatorial Pacific. If two large amplitude anomalies from both hemispheres were to converge on the equator (not seen in this time series), variations of $\partial T/\partial \rho$ would likely be higher amplitude. Assuming that subtropical spiciness anomalies are stochastically generated independent of tropical processes, the possibility for convergence of spiciness within the pycnocline on the equator exists resulting in either large amplitude spiciness or significantly altered $\partial T/\partial \rho$, or both. As these anomalies propagate in the EUC toward the eastern equatorial Pacific, the character of ENSO, specifically the variance of SST, may be affected.

Using the observed variability of $\partial T/\partial \rho$ from Argo float observations as a baseline, spiciness anomalies in the cold tongue region of the eastern equatorial Pacific were simulated using a modified version of the Zebiak-Cane model to determine their effect on ENSO. Variations in $\partial T/\partial \rho$ were slowly introduced to the model over 20,000 years to simulate low-frequency spiciness. The results showed that spiciness anomalies that weaken $\partial T/\partial \rho$ and create a more isothermal pycnocline will dampen the amplitude of ENSO and reduce its variance through weakened thermocline and Ekman feedbacks and a reduction in the non-linearity of the system. As $\partial T/\partial \rho$ increases, so does the non-linearity and the strength of the thermocline feedback term. The dominant balance in the heat budget is between the advection of the anomalous meridional temperature gradient by the mean

meridional currents and the air-sea heat flux. However, the strength of the meridional advection term is determined by the thermocline feedback term through its role in setting up the anomalous meridional temperature gradient. The thermocline feedback term is constrained by equatorial upwelling to only affect SSTA within two to three degrees of the equator, while the meridional advection term distributes this SSTA poleward. The Ekman feedback is also strengthened under increasing $\partial T/\partial \rho$ due to an increase in surface layer divergence from increased zonal wind stress as the thermocline feedback is strengthened. By comparing composites of NINO3 SSTA and the heat budget terms under weak and strong $\partial T/\partial \rho$, it is shown that the growth rate of ENSO increases with increasing $\partial T/\partial \rho$. Distributions of SST anomalies in NINO3 under weak and strong $\partial T/\partial \rho$ conditions show that the departure from normality, a measure of non-linearity, increases with increasing $\partial T/\partial \rho$. However, the center of action of ENSO was shown to be insensitive to changes in $\partial T/\partial \rho$, but this is likely due to the way the model is set up and not indicative of ENSO's response to spiciness. These results support the hypothesis that subsurface spiciness anomalies arriving in the cold tongue region can have a significant affect on ENSO.

In this research, the time mean vertical temperature profile was altered to simulate a change in spiciness. This is acceptable only because the ZC model does not have a density structure and so the thermocline and pycnocline are the same. In reality, this is of course not the case. The true vertical temperature gradient can be decomposed into two components. The first component is the temperature gradient across the pycnocline as we have been using, and the other is the stratification. The dynamics of these components are quite different. $\partial T/\partial \rho$ is controlled by spiciness and is dynamically passive, while $\partial \rho/\partial z$ is proportional to the quasi-geostrophic potential vorticity and is thus affected by planetary wave dynamics. These two variables provide two means of altering the vertical temperature gradient. They also provide another means to modulate the affect of the spiciness anomalies studied here, although the effect of planetary waves would be on a shorter timescale than decadal spiciness anomalies. In addition, $\partial T/\partial \rho$ has both a vertical and horizontal component since the pycnocline is not purely horizontal (and therefore has only the vertical gradient component), as is assumed in this model. This limitation only allows the model to show what happens to one particular aspect of interannual variability. It cannot determine what may happen to the total interannual variability. If the fully density structure is realized, such as in more complex models, the mean state of the horizontal temperature gradient would also be altered and become more important, perhaps altering the zonal SST gradient and surface wind stress.

Another limitation to the model is that the full mixed layer heat budget is not realized and the terms corresponding to anomalous currents advecting anomalous temperature gradients are

omitted. An and Jin (2004) showed that the advection of the anomalous vertical temperature gradient by the anomalous upwelling is the most dominant term in their non-linear dynamic heating (NDH) index. The authors showed that non-linear vertical advection contributed to the strength of El Niño and damped the following La Niña due in part to anomalous subsurface temperatures. Spiciness anomalies could therefore play a role in the strength of the NDH. This effect, however, cannot be studied in the present model as the terms corresponding to NDH are not considered in the heat budget equation.

Also, the mixed layer depth of the model is set to a fixed value of 50 meters. However, the mixed layer depth in the eastern equatorial Pacific is not constant in reality given the large undulations of the pycnocline there. Although it seems as though changes in mixed layer depth and the volume of water in the mixed layer would affect the ability of entrained spiciness to alter SST, Kim, Lee and Fukumori (2007) found that temporal variation in mixed layer depth was not significant in their explicit evaluation of subsurface processes that affect mixed layer temperature in the NINO3 region. In fact, they found that the mixed layer temperature tendency due to entrainment is dominated by large-scale changes in upwelling and subsurface temperature.

In a study of the dominant modes of variability of ENSO, Bejarano and Jin (2008) found that the horizontal advection and thermocline feedbacks play differing roles in the growth and phase transition of the two leading modes, the so-called higher-frequency QB mode and the low-frequency QQ mode. The QQ mode is dominated by the thermocline feedback for both growth and phase transition, while the QB mode has the horizontal advection feedback controlling phase transition. Although spiciness was not shown to alter the dominant period of ENSO in this study, it is plausible that spiciness could influence which mode of variability is likely to dominate through its change in the strength of the feedback mechanisms.

Introducing spiciness to an intermediate coupled model in a damped regime as is done here will not likely produce large changes in the model behavior. The primary result that spiciness can change the variance of ENSO is modest but is interesting nonetheless. It provides a springboard for future researchers to further investigate spiciness as it relates to ENSO. Perhaps a more sophisticated model with fully realized subsurface temperature and sophisticated mixing parameterizations would produce more substantive results and shed more light on how spiciness and ENSO are related.

Bibliography

An, S.-I. and Jin, F.-F. (2001), 'Collective role of thermocline and zonal advective feedbacks in the enso mode*', *Journal of climate* **14**(16), 3421–3432.

An, S.-I. and Wang, B. (2000), 'Interdecadal change of the structure of the enso mode and its impact on the enso frequency*', *Journal of Climate* **13**(12), 2044–2055.

An, S. and Jin, F.-F. (2004), 'Nonlinearity and asymmetry of ENSO', *J. Climate* **17**, 2399–2412.

Ashok, K., Behera, S. K., Rao, S. A., Weng, H. and Yamagata, T. (2007), 'El niño modoki and its possible teleconnection', *Journal of Geophysical Research: Oceans (1978–2012)* **112**(C11).

Battisti, D. (1988), 'The dynamics and thermodynamics of a warming event in a coupled tropical ocean/atmosphere model', *J. Atmos. Sciences* **45**, 2889–2919.

Battisti, D. S. and Hirst, A. C. (1989), 'Interannual variability in a tropical atmosphere-ocean model: Influence of the basic state, ocean geometry and nonlinearity', *Journal of the Atmospheric Sciences* **46**(12), 1687–1712.

Bejarano, L. (2006), Coexistence of leading equatorial coupled modes for ENSO, PhD thesis, Ph. D. Dissertation, Florida State University.

Bejarano, L. and Jin, F.-F. (2008), 'Coexistence of equatorial coupled modes of enso*', *Journal of Climate* **21**(12), 3051–3067.

Blanke, B. and Raynaud, S. (1997), 'Kinematics of the pacific equatorial undercurrent: An eulerian and lagrangian approach from gcm results', *Journal of Physical Oceanography* **27**(6), 1038–1053.

Burgers, G. and Stephenson, D. B. (1999), 'The normality of el niño', *Geophysical Research Letters* **26**(8), 1027–1030.

Deser, C., Alexander, M. A. and Timlin, M. S. (1996), 'Upper-ocean thermal variations in the north pacific during 1970-1991', *Journal of Climate* **9**(8), 1840–1855.

Fedorov, A. V. and Philander, S. G. (2001), 'A stability analysis of tropical ocean-atmosphere interactions: Bridging measurements and theory for el niño', *Journal of Climate* **14**(14), 3086–3101.

Fine, R. A., Lukas, R., Bingham, F. M., Warner, M. J. and Gammon, R. H. (1994), 'The western equatorial pacific: A water mass crossroads', *Journal of Geophysical Research: Oceans (1978–2012)* **99**(C12), 25063–25080.

Giese, B. S., Urizar, S. C. and Fučkar, N. S. (2002), 'Southern hemisphere origins of the 1976 climate shift', *Geophysical Research Letters* **29**(2), 1014.

Goodman, P. J., Hazeleger, W., de Vries, P. and Cane, M. (2005), 'Pathways into the pacific equatorial undercurrent: A trajectory analysis*', *Journal of physical oceanography* **35**(11), 2134–2151.

Gordon, A. L. and Fine, R. A. (1996), 'Pathways of water between the pacific and indian oceans in the indonesian seas', *Nature* **379**(6561), 146–149.

Gouriou, Y. and Toole, J. (1993), 'Mean circulation of the upper layers of the western equatorial pacific ocean', *Journal of Geophysical Research: Oceans (1978–2012)* **98**(C12), 22495–22520.

Gu, D.-F. and Philander, S. (1997), 'Interdecadal climate fluctuations that depend on exchanges between the tropical and extratropics.', *Science* **275**, 805–807.

Huang, R. X. and Wang, Q. (2001), 'Interior communication from the subtropical to the tropical oceans*', *Journal of physical oceanography* **31**(12), 3538–3550.

Jin, F.-F. (1996), 'Tropical ocean-atmosphere interaction, the pacific cold tongue, and the el niño-southern oscillation', *Science* **274**(5284), 76–78.

Jin, F.-F. (1997*a*), 'An equatorial ocean recharge paradigm for enso. part i: Conceptual model', *Journal of the Atmospheric Sciences* **54**(7), 811–829.

Jin, F.-F. (1997*b*), 'An equatorial ocean recharge paradigm for enso. part ii: A stripped-down coupled model', *Journal of the Atmospheric Sciences* **54**(7), 830–847.

Johnson, G. C. (2006), 'Generation and initial evolution of a mode water θ-s anomaly*', *Journal of physical oceanography* **36**(4), 739–751.

Johnson, G. C. and McPhaden, M. J. (1999), 'Interior pycnocline flow from the subtropical to the equatorial pacific ocean*', *Journal of Physical Oceanography* **29**(12), 3073–3089.

Kao, H.-Y. and Yu, J.-Y. (2009), 'Contrasting eastern-pacific and central-pacific types of enso', *Journal of Climate* **22**(3), 615–632.

Kilpatrick, T., Schneider, N. and Di Lorenzo, E. (2011), 'Generation of low-frequency spiciness variability in the thermocline*', *Journal of Physical Oceanography* **41**(2), 365–377.

Kim, S.-B., Lee, T. and Fukumori, I. (2007), 'Mechanisms controlling the interannual variation of mixed layer temperature averaged over the niño-3 region', *Journal of climate* **20**(15), 3822–3843.

Kug, J.-S., Jin, F.-F. and An, S.-I. (2009), 'Two types of el niño events: cold tongue el niño and warm pool el niño', *Journal of Climate* **22**(6), 1499–1515.

Larkin, N. K. and Harrison, D. (2005), 'Global seasonal temperature and precipitation anomalies during el niño autumn and winter', *Geophysical Research Letters* **32**(16), L16705.

Lu, P. and McCreary Jr, J. P. (1995), 'Influence of the itcz on the flow of thermocline water from the subtropical to the equatorial pacific ocean', *Journal of physical oceanography* **25**(12), 3076–3088.

Luo, Y., Rothstein, L. M., Zhang, R.-H. and Busalacchi, A. J. (2005), 'On the connection between south pacific subtropical spiciness anomalies and decadal equatorial variability in an ocean general circulation model', *Journal of Geophysical Research: Oceans (1978–2012)* **110**(C10).

McCreary, J. and Lu, P. (1994), ' Interaction between the subtropical and the equatorial ocean circulations: The subtropical cell.', *J. Phys. Oceanogr.* **24**, 466–497.

Moore, A. M. and Kleeman, R. (1999), 'Stochastic forcing of enso by the intraseasonal oscillation', *Journal of Climate* **12**(5), 1199–1220.

Munk, W. (1981), 'Internal waves and small-scale processes', *Evolution of physical oceanography* pp. 264–291.

Nonaka, M. and Sasaki, H. (2007), 'Formation mechanism for isopycnal temperature-salinity anomalies propagating from the eastern south pacific to the equatorial region', *Journal of climate* **20**(7), 1305–1315.

Nonaka, M., Xie, S.-P. and Takeuchi, K. (2000), 'Equatorward spreading of a passive tracer with application to north pacific interdecadal temperature variations', *Journal of oceanography* **56**(2), 173–183.

Rasmusson, E. M. and Carpenter, T. H. (1982), 'Variations in tropical sea surface temperature and surface wind fields associated with the southern oscillation/el niño', *Monthly Weather Review* **110**(5), 354–384.

Sasaki, Y. N., Schneider, N., Maximenko, N. and Lebedev, K. (2010), 'Observational evidence for propagation of decadal spiciness anomalies in the north pacific', *Geophysical Research Letters* **37**(7).

Schneider, N. (2000), 'A decadal spiciness mode in the tropics', *Geophys. Res. Lett.* **217**, 257–260.

Schneider, N. (2004), 'The response of tropical climate to the equatorial emergence of spiciness anomalies', *J. Climate* **17**, 1083–1095.

Schneider, N., Miller, A. J., Alexander, M. A. and Deser, C. (1999), 'Subduction of decadal north pacific temperature anomalies: Observations and dynamics', *Journal of Physical Oceanography* **29**(5), 1056–1070.

Syu, H.-H., Neelin, J. D. and Gutzler, D. (1995), 'Seasonal and interannual variability in a hybrid coupled gcm', *Journal of climate* **8**(9), 2121–2143.

Taguchi, B. and Schneider, N. (2013), 'Origin of decadal-scale, eastward-propagating heat content anoma- lies in the north pacific', *Journal of Climate, submitted* .

Tailleux, R., Lazar, A. and Reason, C. (2005), 'Physics and dynamics of density compensated temperature and salinity anomalies. part i: Theory', *J. Phys. Oceanogr.* **35**, 849–864.

Torrence, C. and Compo, G. P. (1998), 'A practical guide to wavelet analysis', *Bulletin of the American Meteorological society* **79**(1), 61–78.

Trenberth, K. E. and Hoar, T. J. (1996), 'The 1990–1995 el niño-southern oscillation event: Longest on record', *Geophysical Research Letters* **23**(1), 57–60.

Trenberth, K. E. and Stepaniak, D. P. (2001), 'Indices of el niño evolution', *Journal of Climate* **14**(8), 1697–1701.

Vincent, E. M., Lengaigne, M., Menkes, C. E., Jourdain, N. C., Marchesiello, P. and Madec, G. (2011), 'Interannual variability of the south pacific convergence zone and implications for tropical cyclone genesis', *Climate dynamics* **36**(9-10), 1881–1896.

Wang, Q. and Huang, R. X. (2005), 'Decadal variability of pycnocline flows from the subtropical to the equatorial pacific*', *Journal of physical oceanography* **35**(10), 1861–1875.

Yeager, S. G. and Large, W. G. (2004), 'Late winter generation of spiciness on subducted isopycnals', *J. Phys. Oceanogr.* **34**, 1528–1547.

Yeager, S. G. and Large, W. G. (2007), 'Observational evidence of winter spice injection', *Journal of Physical Oceanography* **37**(12), 2895–2919.

Yu, J.-Y. and Kao, H.-Y. (2007), 'Decadal changes of enso persistence barrier in sst and ocean heat content indices: 1958–2001', *Journal of Geophysical Research: Atmospheres (1984–2012)* **112**(D13).

Zebiak, S. E. and Cane, M. A. (1987), 'A model el niñ-southern oscillation', *Monthly Weather Review* **115**(10), 2262–2278.

Zhang, R.-H., Kagimoto, T. and Zebiak, S. E. (2001), 'Subduction of decadal north pacific thermal anomalies in an ocean gcm', *Geophysical research letters* **28**(12), 2449–2452.